Lattice QCD study for the relation between confinement and chiral symmetry breaking

Takahiro Doi
Department of Physics, Kyoto University

February 3, 2017

Abstract

It is one of the most important problems in particle and nuclear physics to understand the nonperturbative properties of QCD, such as confinement and chiral symmetry breaking, including these relation. In spite of numerous efforts, these properties have not been sufficiently understood yet. The main goal of this thesis is to understand the relation between quark-confinement and chiral symmetry breaking in QCD, both analytically and numerically from the first principle. To that end, several analytical relations are derived using the lattice QCD formalism, connecting order parameters for quark-confinement and the Dirac eigenmodes. We consider the Polyakov loop, its fluctuations, and the Wilson loop as the order parameters for quark-confinement. According to the Banks-Casher relation, the low-lying eigenmodes of the Dirac operator have the dominant contributions to the chiral condensate which is the order parameter for chiral symmetry breaking. From these analytical formulae, it is proven that the low-lying Dirac modes have little contributions to the order parameters for quark-confinement. From the analysis for the Dirac-spectrum representation of the Polyakov loop, a new symmetry, referred to as the "positive/negative symmetry," is found in the Dirac-mode matrix element of the link-variable operator, and it leads to the zero value of the Polyakov loop in the confinement phase. However, in the deconfinement phase, the positive/negative symmetry is broken, and the Polyakov loop has the non-zero value. Although the analytical relations connecting the Polyakov loop and the eigenmodes of the overlap-Dirac operator seem difficult to derive, we can show that the confinement property such as the value of the Polyakov loop, is independent of the density of low-lying overlap-Dirac modes. Then, we conclude that there is no direct one-to-one correspondence between quark-confinement and chiral symmetry breaking in QCD.

Contents

Chapter 1

Introduction

1.1 QCD

The fundamental theory of strong interaction is Quantum chromodynamics (QCD)[1, 2]. The QCD lagrangian is

$$\mathcal{L}_{\rm QCD} = -\frac{1}{4} G^{a\mu\nu} G^{a}{}_{\mu\nu} + \bar{q}(i\gamma^{\mu} D_{\mu} - m_q)q. \tag{1.1}$$

where the field strength $G^{a}{}_{\mu\nu}$ the covariant derivative D_{μ} are defined as

$$G^{a}{}_{\mu\nu} = \partial_{\mu} A^{a}_{\nu} - \partial_{\nu} A^{a}_{\mu} - g f^{abc} A^{b}_{\mu} A^{c}_{\nu}, \tag{1.2}$$

$$D_{\mu} = \partial_{\mu} + i g A^{a}_{\mu} T^{a}. \tag{1.3}$$

QCD is a non-Abelian gauge theory with the SU(3) gauge symmetry and its gauge coupling is denoted as g. The quark field $q^{\alpha i f}$ has the spinor index ($\alpha = 1, 2, 3, 4$), the color index of the fundamental representation of SU(3) ($i = 1, 2, 3$), and the flavor index ($f = 1, \cdots, N_f$). The gauge field A_{μ} is called gluon, and has the index of Lorentz vector ($\mu = 1, 2, 3, 4$), and the color index of the adjoint representation of SU(3) ($a = 1, \cdots, 8$). m_q is current quark mass. One of the most important feature of QCD is that QCD is non-Abelian gauge theory. When gauge group is non-Abelian, non-linear terms of gauge fields appear in the fields strength, Eq. (1.2), because the structure constant is nonzero: $f^{abc} \neq 0$. These non-linear terms leads the self-interaction terms in the lagrangian, Eq. (1.1). Because of these self-interaction terms, QCD is asymptotic free [3, 4]. In fact, the running coupling constant of the SU($N_{\rm c}$) non-Abelian theory with massless N_f fermions is calculated as

$$\alpha_{\rm s}(Q^2) = \frac{g^2(Q)}{4\pi} = \frac{12\pi}{11 N_{\rm c} - 2 N_{\rm f}} \frac{1}{\ln(\frac{Q^2}{\Lambda^2_{\rm QCD}})} \tag{1.4}$$

up to the order of 1-loop. $\Lambda_{\rm QCD}$ is the typical scale of QCD and should be determined from experiment. With the parameter set of QCD, QCD is asymptotic free. In other words, the coupling constant becomes weak at high energy scale or short distance. Then, low-energy QCD is practically difficult to be investigated since the perturbation theory cannot be used due to the strong coupling. However, low-energy QCD is phenomenologically very interesting because the nature of the strong coupling leads various non-perturbative phenomena, such as confinement and chiral symmetry breaking. These phenomena are main targets of this thesis.

1.2 Confinement

Confinement is one of the most characteristic phenomena in QCD. The most general statement of confinement hypothesis is that color charged states cannot be observed and only color singlet states can be observed [5]. For example, in QCD with Nc = 3, quark(q), gluon and diquark(qq) are color charged, and meson($\bar{q}q$), baryon(qqq), and glueball are color-singlet states. At the present, although nobody has succeeded in proving the confinement, or even quark-confinement from the first-principle, there is no experiment to detect any color charged states. In particular, the quark-confinement has been most intensively investigated, and several scenarios for (quark-)confinement are suggested. In the following, we review them.

Figure 1.1: The schematic figure for the flux tube between quark-antiquark pair in the QCD vacuum.

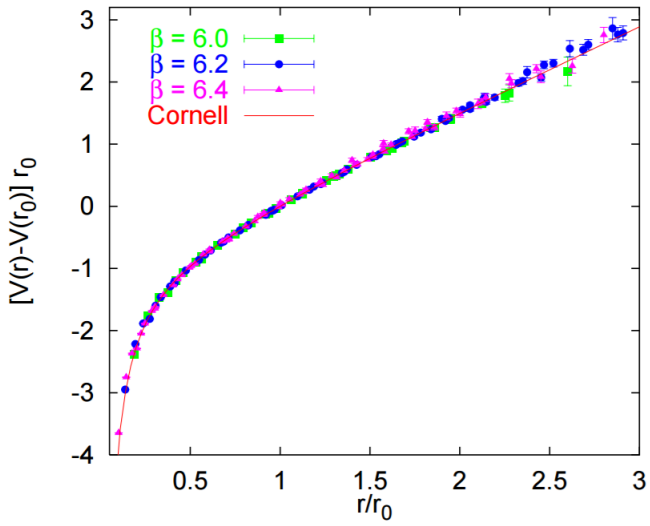

Figure 1.2: The interquark potential calculated from the Wilson loop in the lattice unit. Each point is obtained by lattice QCD calculation, and it is well fit with the Cornell potential (1.5), denoted as the solid line. The figure is taken from Ref. [8].

The linear potential between quark and anti-quark gives the simplest explanation for quark-confinement [6, 7, 8]. When a quark and an anti-quark are put in the QCD vacuum, the color electric fields generate the 1-dimensional gluonic flux tube between them, shown in Fig. 1.1. It is essentially different from the electric fields in QED, where electrons are not confined. The 1-dimensional flux tube gives the confinement potential for the system. In fact, as shown in Fig. 1.2, when R is the distance of the quark and anti-quark, the interquark potential $V(R)$ is calculated in the lattice QCD from the Wilson loop and it can be very well fit with the Cornell potential

$$V(R) = -A/R + \sigma R + C \tag{1.5}$$

where A, σ, and C are fitting parameters. The coefficient σ of the linear term is called string tension because it gives the strength of the linear-confining force. The Coulomb-type potential at short distance can be understood from the asymptotic freedom because the perturbative theory is applicable there. This potential shows that the interquark potential $V(R)$ infinitely increases as the distance R becomes larger. Thus, a single quark cannot exist. However, the above discussion is based on the assumption that the quark mass is infinitely heavy. Then, in the case of quark with finite mass, when the

distance R increases and the interquark potential $V(R)$ exceeds a threshold of pair-creation of quark and anti-quark, a new pair of quark and anti-quark is generated. In the case of a qqq system, the shape of the flux tube between quarks is Y-type [9, 10, 11]. In fact, the flux tube is confirmed by the lattice QCD calculation, shown in Fig. 1.3. At high temperature, the color con-

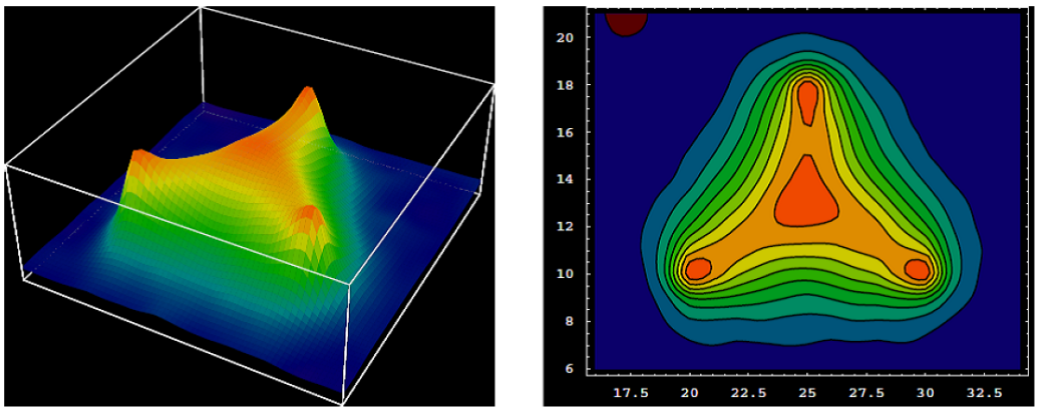

Figure 1.3: The Y-type flux tube generated in the 3 quark system. It is calculated from the lattice QCD simulations. The figure is taken from Ref. [9].

finement does not occur, and the system is changed from the confinement phase to the deconfinement phase. In the deconfinement phase, the system is considered to be a gas-like state of quarks and gluons. As a order parameter for the quark-deconfinement transition, the Polyakov loop has been strongly investigated. The Polyakov loop is related to the energy of the system with a single quark [12, 13]. Thus, the Polyakov loop distinguishes the confinement and deconfinement phases because the energy is infinite if the quark is confined and it is finite if the quark is deconfined. The Polyakov loop is one of the main observables to study in this thesis, and then we discuss the properties of it in the subsequent sections.

A candidate of the mechanism for the generation of the 1-dimensional flux tube is the dual superconductivity picture [15, 16, 17]. This picture of the confinement is an analogy of the type-II superconductor. In the superconductivity phase of the type-II superconductor, magnetic field is squeezed and 1-dimensional magnetic flux is generated. Although this situation is similar with the confinement, there are of course critical differences. The most important difference is that the electric field should be squeezed in QCD,

not magnetic field. The roles of the electric and magnetic fields in the superconductor are exchanged in the non-perturbative vacuum of QCD(QCD vacuum). This dual-superconductivity picture expects that the QCD vacuum is dual-superconductor, where "dual" means the duality of the electric and magnetic fields. However, the duality in QCD is difficult to understand because QCD is SU(3) gauge theory. In fact, while the magnetic monopole can be defined in Abelian gauge theory, it is difficult to be define in non-Abelian gauge theories, such as QCD. This problem is avoided by the gauge fixing. For example, using the maximally Abelian gauge (MAG), the QCD monopole appears as a topological object, and it is important for the non-perturbative phenomena, such as confinement, chiral symmetry breaking. This picture is confirmed in the dual Ginzburg-Landau theory [18] and the lattice QCD [19, 20, 21].

As a method to define the magnetic monopole in QCD without gauge fixing, Cho-Faddeev-Niemi decomposition is suggested [22, 23, 24]. The confinement phenomenon can be explained by the condensation of the magnetic monopole appearing due to the decomposition. In fact, there is the lattice QCD study to support this picture [24].

There is some studies on the mechanism for confinement based on the BRST formalism by fixing the covariant gauge [25]. It is shown that physical state is the BRST singlet state. Motivated by this fact, it is expected that color charged states are not BRST singlet states, namely physical states. This theory is called Kugo-Ojima formalism, and it provides a general picture of color-confinement. However, this picture is found to be not complete by the lattice QCD calculation [26].

The truncated Schwinger-Dyson equation is useful method to analyze the properties of the QCD vacuum. Using the Schwinger-Dyson equation, it is suggested that The quark scalar density is sensitive to the strength of the confining force [27, 28].

1.3 Chiral Symmetry breaking

Chiral symmetry breaking is the phenomenon that the chiral symmetry $\mathrm{SU}(N_f)_\mathrm{L} \times \mathrm{SU}(N_f)_\mathrm{R}$ of the QCD lagrangian (1.1) with the chiral limit ($m_q \to 0$) is spontaneously broken in the vacuum [29, 30, 31]. As a result, $(N_f^2 - 1)$ massless Nambu-Goldstone bosons appear and quark obtains constituent quark mass. Since the quark mass is nonzero $m_q \neq 0$ in the real world, it is said that chiral symmetry is approximately broken. $\mathrm{SU}(N_f)_\mathrm{L} \times \mathrm{SU}(N_f)_\mathrm{R}$ chiral transformation is two independent $\mathrm{SU}(N_f)$ transformation to the left-handed component of a quark field $q_{\mathrm{L},f} \equiv (\frac{1-\gamma_5}{2})q_f$ and the right-handed

component $q_{\mathrm{R},f} \equiv (\frac{1+\gamma_5}{2})q_f$ as

$$q_{\mathrm{L},f} \to q'_{\mathrm{L},f} = U(\theta_{\mathrm{L}})_{ff'} q_{\mathrm{L},f'} \ , \quad U(\theta_{\mathrm{L}})_{ff'} = \exp(i\theta^a_{\mathrm{L}} T^a) \in \mathrm{SU}(N_{\mathrm{f}})_{\mathrm{L}} \tag{1.6}$$

$$q_{\mathrm{R},f} \to q'_{\mathrm{R},f} = U(\theta_{\mathrm{R}})_{ff'} q_{\mathrm{R},f'} \ , \quad U(\theta_{\mathrm{R}})_{ff'} = \exp(i\theta^a_{\mathrm{R}} T^a) \in \mathrm{SU}(N_{\mathrm{f}})_{\mathrm{R}} \tag{1.7}$$

θ^a_{L} and θ^a_{R} are independent parameters. This chiral transformation can be decomposed to the vector and axial transformations.

$$q_f \to q'_f = U(\theta_{\mathrm{V}})_{ff'} q_{f'} \ , \quad U(\theta_{\mathrm{V}})_{ff'} = \exp(i\theta^a_{\mathrm{V}} T^a) \in \mathrm{SU}(N_{\mathrm{f}}) \tag{1.8}$$

$$q_f \to q'_f = U(\theta_{\mathrm{A}})_{ff'} q_{f'} \ , \quad U(\theta_{\mathrm{A}})_{ff'} = \exp(i\gamma_5\theta^a_{\mathrm{A}} T^a) \tag{1.9}$$

The vector transformation corresponds to the chiral transformation with same parameters ($\theta_{\mathrm{L}} = \theta_{\mathrm{R}} = \theta_{\mathrm{V}}$) for the right- and left-handed components. The axial transformation corresponds to the chiral transformation with the opposite parameters ($\theta_{\mathrm{L}} = -\theta_{\mathrm{R}} = -\theta_{\mathrm{A}}$). Although the QCD lagrangian is invariant under the vector transformation even with massive quarks with $m_q \neq 0$, the invariance under the axial transformation is valid for the massless case. Then, the chiral symmetry is essentially the invariance under the axial transformation.

The QCD lagrangian (1.1) has the chiral symmetry in the chiral limit ($m_q \to 0$). Since the quarks have finite masses, the chiral symmetry is not the exact symmetry of QCD. However, the chiral symmetry is approximate symmetry in the u and d sectors because these masses are smaller than the QCD scale Λ_{QCD}. Therefore, if the chiral symmetry is realized at the level of states, the symmetry should appear in the hadron spectrum. However, experimental results does not indicate the symmetry, and then it is called as chiral symmetry breaking. In fact, the chiral symmetry is spontaneously broken from $\mathrm{SU}(N_f)_{\mathrm{L}} \times \mathrm{SU}(Nf)_{\mathrm{R}}$ to $\mathrm{SU}(N_f)_{\mathrm{V}}$. The order parameter of the chiral symmetry breaking is the chiral condensate $\langle\bar{q}q\rangle$. In the following, $\langle\bar{q}q\rangle$ means the chiral condensate per a flavor.

Since the chiral symmetry is the global symmetry, the Nambu-Goldstone bosons (NG bosons) appear followed by the Nambu-Goldstone theorem. In fact, the pions are the lightest hadron, and they can be regarded as the NG bosons associated with the SU(2) chiral symmetry of the u and d sectors. The reason why it has the finite mass is that the u and d quarks have the finite current quark masses. When a global symmetry is spontaneously broken, some observables related to the NG boson are determined at low-energy. This is low-energy theorem [1]. For example, the Gell-Mann-Oaks-Renner relation

$$m_\pi^2 f_\pi^2 = -2m_q\langle\bar{q}q\rangle \tag{1.10}$$

and the Goldberger-Treiman relation

$$g_{\pi \mathrm{N}} f_\pi = m_{\mathrm{N}} g_{\mathrm{A}} \tag{1.11}$$

are the examples of the low-energy theorem. The pion decay constant $f_\pi = 93$ MeV, the pion mass m_π, the nucleon mass m_N, the $\pi - N$ coupling constant $g_{\pi N}$, and the axial charge g_A are important parameters of the low-energy QCD.

1.3.1 Banks-Casher relation

The order parameter of the chiral symmetry breaking is the chiral condensate $\langle \bar{q} q \rangle$. The chiral condensate is related with the zero-mode density of the Dirac operator known as the Banks-Casher relation [32]. Since the Banks-Casher relation plays a very important role in this study, we show the derivation of the relation in this subsection. We consider the euclidean QCD. The gamma matrices are taken as hermit ($\gamma_\mu^\dagger = \gamma_\mu$). The eigenvalue equation of the Dirac operator $\not{D}$ is shown as

$$\not{D} |n\rangle = i\lambda_n |n\rangle. \tag{1.12}$$

Since $\not{D}$ is anti-hermit, the eigenvalue is pure imaginary and λ_n is real. $|n\rangle$ is the eigenstate. In the following, we call these modes as Dirac modes. The Dirac mode is orthonormal basis:

$$\langle m|n\rangle = \delta_{mn}. \tag{1.13}$$

The Dirac operator anti-commutes the γ_5 as

$$\{\not{D}, \gamma_5\} = 0. \tag{1.14}$$

This fact means that the state $\gamma_5|n\rangle$ has the eigenvalue $-i\lambda_n$, which is opposite sign of the eigenvalue of the state $|n\rangle$.

$$\not{D}\gamma_5|n\rangle = -\gamma_5 \not{D}|n\rangle = -\gamma_5 i\lambda_n |n\rangle = -i\lambda_n \gamma_5 |n\rangle. \tag{1.15}$$

Now we can derive the Banks-Casher relation by deforming the chiral

condensate $\langle\bar{q}q\rangle$ in the following.

$$\langle\bar{q}q\rangle = \frac{1}{V}\int dx \sum_{\alpha,i}\langle\bar{q}^{\alpha i}(x)q^{\alpha i}(x)\rangle \tag{1.16}$$

$$= -\frac{1}{V}\left\langle \mathrm{Tr}_{c,\gamma}\left(\frac{1}{\not{D}+m}\right)\right\rangle \tag{1.17}$$

$$= -\frac{1}{V}\left\langle \sum_n \langle n|\frac{1}{\not{D}+m}|n\rangle\right\rangle \tag{1.18}$$

$$= -\frac{1}{V}\left\langle \sum_n \frac{1}{i\lambda_n+m}\right\rangle \tag{1.19}$$

$$= -\frac{1}{V}\int_{-\infty}^{\infty} d\lambda \frac{1}{i\lambda+m}\left\langle \sum_n \delta(\lambda-\lambda_n)\right\rangle \tag{1.20}$$

$$= -\frac{1}{i}\int_{-\infty}^{\infty} d\lambda \frac{1}{\lambda-im}\langle\rho(\lambda)\rangle \quad (\rho(\lambda)\equiv\frac{1}{V}\sum_n\delta(\lambda-\lambda_n)) \tag{1.21}$$

$$\to -\frac{1}{i}\int_{-\infty}^{\infty} d\lambda \langle\rho(\lambda)\rangle\left(\mathrm{P}\frac{1}{\lambda}+i\pi\delta(\lambda)\right) \quad (m\to 0) \tag{1.22}$$

$$\to -\pi\langle\rho(0)\rangle \quad (V\to\infty) \tag{1.23}$$

We assume the homogeneous condensate $\langle\bar{q}q\rangle$. $\mathrm{Tr}_{c,\gamma}$ is the functional trace over the indices of space-time, color, and spinor. In Eq. (1.18), the Dirac modes are taken as the basis of the functional trace. The Dirac eigenvalue density $\rho(\lambda)$ is defined as

$$\rho(\lambda) \equiv \frac{1}{V}\sum_n \delta(\lambda-\lambda_n) \tag{1.24}$$

and it becomes a smooth function at the thermodynamics limit $V\to\infty$. P in Eq. (1.22) denotes the principal value integral, and we use the relation between the delta function and the principal value integral

$$\lim_{\epsilon\to 0}\frac{1}{x+i\epsilon} = \mathrm{P}\frac{1}{x} - i\pi\delta(x). \tag{1.25}$$

From Eq. (1.15), $\rho(\lambda)$ is even function, and then the first term of Eq. (1.22) vanishes. Therefore, the Banks-Casher relation is expressed as

$$\langle\bar{q}q\rangle = -\lim_{m\to 0}\lim_{V\to\infty}\pi\langle\rho(0)\rangle. \tag{1.26}$$

The Banks-Casher relation means that the density of the Dirac zero modes gives the chiral condensate. In other words, the Dirac zero modes are the important modes for chiral symmetry breaking. This fact is one of the most important points of this thesis.

1.4 Lattice QCD

In this section, we review the basics of the lattice QCD. The lattice QCD is the discretized QCD respecting the gauge symmetry on the euclidean space-time [12, 33, 34]. Although the QCD lagrangian is defined on the Minkowski space, the euclidean QCD can be obtained by the Wick rotation. The action and the lagrangian of the euclidean QCD are

$$S^{\mathrm{E}}_{\mathrm{QCD}} = \int d^4x^{\mathrm{E}} \mathcal{L}^{\mathrm{E}}_{\mathrm{QCD}} \tag{1.27}$$

$$\mathcal{L}^{\mathrm{E}}_{\mathrm{QCD}} = \frac{1}{4}(G^{\mathrm{E}})_{a\mu\nu}(G^{\mathrm{E}})_{a\mu\nu} + \bar{q}(\gamma^{\mathrm{E}}_{\mu} D^{\mathrm{E}}_{\mu} + m_q)q \tag{1.28}$$

In this thesis, the gamma matrices are taken as hermit and satisfy the anti-commutator relation

$$\{\gamma^E_\mu, \gamma^E_\nu\} = 2\delta_{\mu\nu} \tag{1.29}$$

$$(\gamma^E_\mu)^\dagger = \gamma^E_\mu \tag{1.30}$$

After Wick rotation, the euclidean generating functional is

$$Z = \int \mathcal{D}A\mathcal{D}\bar{q}\mathcal{D}q \mathrm{e}^{-S^{\mathrm{E}}_{\mathrm{QCD}}}. \tag{1.31}$$

In the following, we suppress the Euclidean index "E".

The lattice QCD is discretized euclidean QCD respecting the SU(3) gauge theory. There are multiple lattice actions, corresponding to associated discretization, and they have the same continuum limit. In this thesis, we consider the plaquette action for the gauge sector and the Wilson, Wilson-clover, the overlap actions for the fermion sector.

We use a standard square lattice with spacing a, and the notation of sites $s = (s_1, s_2, s_3, s_4)$ ($s_\mu = 1, 2, \cdots, N_\mu$), and link-variables $U_\mu(s) = \mathrm{e}^{iagA_\mu(s)}$ with gauge fields $A_\mu(s) \in su(N_c)$ and gauge coupling g. The link variable $U_\mu(s)$ has the relation with the gauge variable $A_\mu(s)$ as

$$U_\mu(s) = \mathrm{e}^{iagA_\mu(s)}. \tag{1.32}$$

The gauge transformation on the lattice is

$$q(s) \to q'(s) = \Omega(s)q(s) \tag{1.33}$$

$$U_\mu(s) \to U'_\mu(s) = \Omega(s)U_\mu(s)\Omega(s+\hat{\mu})^\dagger \tag{1.34}$$

$$\Omega(s) \in \mathrm{SU}(3), \tag{1.35}$$

where $\hat{\mu}$ is the unit vector with the direction μ satisfying $|\hat{\mu}| = a$. This transformation is the gauge theory in the continuum theory at the continuum limit $a \to 0$.

The plaquette action for the gauge sector is

$$S_g = \beta \sum_s \sum_{\mu>\nu} \left[1 - \frac{1}{2N_c} \mathrm{Tr}(U_{\mu\nu}(s) + U_{\mu\nu}(s)^\dagger) \right], \tag{1.36}$$

where the plaquette $U_{\mu\nu}(s)$ is defined as

$$U_{\mu\nu}(s) = U_\mu(s) U_\nu(s+\hat{\mu}) U_\mu(s+\hat{\nu})^\dagger U_\nu(s)^\dagger, \tag{1.37}$$

and has the connection with the field strength $G_{\mu\nu}$ near the continuum limit.

$$U_{\mu\nu}(s) = \exp\left[i a^2 g G_{\mu\nu} + \mathcal{O}(a^3) \right]. \tag{1.38}$$

The plaquette action approaches the continuum kinetic term of the gauge field with $\mathcal{O}(a^2)$.

The fermionic action $a^4 \sum_s \bar{q}(s) \left(D_{\mathrm{Lat}} + m \right) q(s)$ on the lattice is more complicated than the gauge sector, where D_{Lat} is the Dirac operator on the lattice. If the Dirac operator is naively discretized respecting all the symmetries of QCD, unphysical modes appear and the number of the doubler modes is 2^d on a $d-$dimensional lattice. This problem is referred to as the fermion doubling problem. The number of low-energy modes is important for the low-energy dynamics. Thus the doubling problem should be avoided by some way. However, it is proven that the fermion doubling problem cannot be solved if the lattice fermionic action satisfies the conditions

- translational invariance
- chiral symmetry
- hermiticity
- bilinear form of quark field
- locality

known as Nielsen-Ninomiya theorem [12, 35, 36]. Then, the doubling problem is usually avoided by breaking the condition: chiral symmetry. The concrete method to avoid the doubling problem is discussed in the chapter 3.

1.5 Motivation and Outline of this thesis

As reviewed above, the non-perturbative phenomena are important for the dynamics of QCD at low energy. In this study, we focus the relations between them, in particular quark-confinement and chiral symmetry breaking. In the following, we explain our motivation with previous works and outline of this thesis.

Whether quarks are confined or deconfined, and whether the chiral symmetry is broken or restored determine the phases of QCD, such as the hadronic phase where color is confined and chiral symmetry is broken, the quark gluon plasma where color is deconfined and chiral symmetry is restored, and the color-superconductivity phase where the Cooper pair of the quarks is condensed [37, 38, 39]. The diagram explaining the phases of QCD at finite temperature T and chemical potential μ is referred to as the QCD phase diagram, and it has been intensively investigated by mainly effective models of QCD [40, 41]. An expected QCD phase diagram is shown in Fig. 1.4. However, nobody has not drown the full range of the QCD phase diagram based on the first principle[1] because the Monte-Carlo simulation for the lattice QCD is quite difficult to perform at finite chemical potential. This is referred to as the sign problem, and has not been fully solved yet [42, 43, 44, 45].

In addition to the sign problem, there is a problem on the relation between confinement and chiral symmetry breaking in the past studies on the QCD phase diagram. In fact, color-deconfinement and chiral restoration are supposed to be simultaneously happened. However, this is nontrivial assumption, and that is what we will show in this thesis. Then, the relation between these nonperturbative phenomena is important topic.

Although that relation has been studied [46, 47, 48, 49, 50, 51, 52, 53], it has not been sufficiently understood yet. In many lattice-QCD calculations at finite temperature, both quark deconfinement and chiral restoration occur in the same temperature range [54, 55]. Moreover, after removal of the QCD monopole, quark-confinement and chiral symmetry breaking simultaneously disappear [56, 57]. However, these result does not necessarily imply that quark-confinement and chiral symmetry breaking are strongly correlated, as there are some opposite results. For example, there are calculations showing that the deconfinement crossover temperature is significantly higher than the chiral crossover temperature for physical values of quark masses [58, 59, 60]. In addition, some numerical analysis suggest that after removing the low-

[1] In the cases of finite temperature with zero chemical potential, color SU(2), imaginary chemical potential, or isospin chemical potential, the Monte-Carlo simulation can be performed.

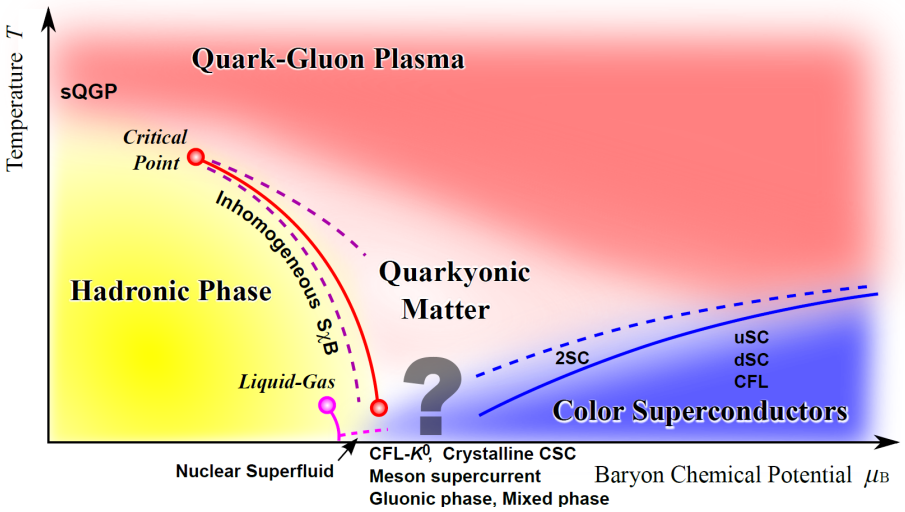

Figure 1.4: An expected QCD phase diagram based on several studies using effective models. The figure is taken from Ref. [41].

lying Dirac modes, "hadrons" as bound state of quarks and gluons can be still observed on the lattice [50], and the Polyakov loop and the srting tension are almost unchanged [51, 52]. The main goal of this study is to understand the relation between confinement and chiral symmetry breaking based on the first principle, namely the lattice QCD, both analytically and numerically.

In the following, the outline of this thesis is shown. In Chapter 2, we discuss the relation between confinement and chiral symmetry breaking by deriving the analytical formulae connecting the Dirac eigenmodes and the order parameters for quark-confinement, such as the Polyakov loop, the Polyakov loop fluctuations, and the Wilson loop. Then, we analytically and numerically observe the negligible contributions from the low-lying Dirac modes to these order parameters. However, the argument in Chapter 2 has a problem about the fermion doubler modes on the lattice. Then, in chapter 3, the above discussion is generalized to the chiral fermion on the lattice. Finally, in Chapter 4 we draw some conclusions and present an outlook.

Chapter 2

Relation between confinement and chiral symmetry breaking

2.1 Polyakov loop

In this section, we discuss the relation between confinement and chiral symmetry breaking in QCD by deriving several analytical formulae connecting the Polyakov loop and the Dirac eigenmodes.

Operator formalism & Dirac modes on lattice

In order to derive the relations, we first prepare the operator formalism and the Dirac modes in the SU(N_c) lattice QCD [51, 61].

The link-variable operator $\hat{U}_{\pm\mu}$ is defined as the matrix element

$$\langle s|\hat{U}_{\pm\mu}|s'\rangle = U_{\pm\mu}(s)\delta_{s\pm\hat{\mu},s'}, \tag{2.1}$$

where s denotes the site on the lattice and $\hat{\mu}$ is the unit vector in direction μ in the lattice unit. Using the link-variable operator, the several quantity can be redefined. The covariant derivative operator $\hat{D}_\mu$ on the lattice expressed as

$$\hat{D}_\mu = \frac{1}{2a}(\hat{U}_\mu - \hat{U}_{-\mu}) \tag{2.2}$$

corresponding to the matrix element (3.2). And then the naive Dirac operator on the lattice $\hat{\not{D}}$ can be given by

$$\hat{\not{D}} = \gamma_\mu \hat{D}_\mu = \frac{1}{2a}\sum_{\mu=1}^{4}\gamma_\mu(\hat{U}_\mu - \hat{U}_{-\mu}). \tag{2.3}$$

Corresponding to Eqs. (1.12), (1.13), and (1.14), the eigenvalue equation of the naive Dirac operator is

$$\hat{\not{D}}|n\rangle = i\lambda_n|n\rangle \tag{2.4}$$

with the completeness relation the chiral symmetry

$$\langle m|n\rangle = \delta_{mn} \tag{2.5}$$

$$\{\not{D}, \gamma_5\} = 0. \tag{2.6}$$

The coordinate representation of the eigenstate is expressed as the eigenfunction $\psi_n(s) \equiv \langle s|n\rangle$, and the explicit form for the Dirac eigenvalue equation is written by

$$\frac{1}{2a}\sum_{\mu=1}^{4}\gamma_\mu[U_\mu(s)\psi_n(s+\hat{\mu}) - U_{-\mu}(s)\psi_n(s-\hat{\mu})] = i\lambda_n\psi_n(s). \tag{2.7}$$

Here, the link-variables are given by the Monte-Carlo simulation in the lattice QCD, and then the eigenfunction can be directly calculated. The Dirac eigenfunction $\psi_n(s)$ has an irrelevant phase factor $\mathrm{e}^{i\varphi_n[V]}$ because $\psi_n(s)$ is gauge-transformed as

$$\psi_n(s) \to V(s)\psi_n(s), \tag{2.8}$$

by the gauge transformation of $U_\mu(s) \to V(s)U_\mu(s)V^\dagger(s+\hat{\mu})$. The transformation law is the same as that of the quark field. This mode-dependent global phase factor corresponds to arbitrariness of the phase in the basis $|n\rangle$ [51].

The antiperiodic boundary condition for the imaginary-time direction is necessary for the finite-temperature formalism. Thus, we impose the antiperiodic boundary condition to the link-variable operator as

$$\begin{aligned}\langle \mathbf{s}, N_\tau|\hat{U}_4|\mathbf{s}, 1\rangle &= -U_4(\mathbf{s}, N_\tau), \\ \langle \mathbf{s}, 1|\hat{U}_{-4}|\mathbf{s}, N_\tau\rangle &= -U_{-4}(\mathbf{s}, 1) = -U_4^\dagger(\mathbf{s}, N_\tau).\end{aligned} \tag{2.9}$$

at the temporal boundary $t = N_\tau(= 0)$ [62]. This temporal boundary condition does not influence the plaquette action and the clover term because they are constituted of the spatial loop of the link-variables. If a loop crosses the temporal boundary, the minus sign appear twice and they are canceled in the loop.

Next, the Polyakov loop, which is an order parameter for the quark-confinement, is expressed as

$$L = -\frac{1}{N_c V}\mathrm{Tr}_c\{\hat{U}_4^{N_\tau}\} = \frac{1}{N_c V}\sum_s \mathrm{tr}_c\{\prod_{n=0}^{N_t-1} U_4(s+n\hat{4})\}, \tag{2.10}$$

using the link-variable operators, where Tr_c is the functional trace, $\mathrm{Tr}_c \equiv \sum_s \mathrm{tr}_c$, taken over the indeces of sites and colors. The minus sign in the definition comes from the additional minus on $U_4(\mathbf{s}, N_\tau)$ in Eq.(2.9).

We discuss the property of the Dirac-mode matrix element of the link-variable operator $\langle m|\hat{U}_\mu|n\rangle$. It can be explicitly written as

$$\begin{aligned}\langle m|\hat{U}_\mu|n\rangle &= \sum_s \langle m|s\rangle\langle s|\hat{U}_\mu|s+\hat{\mu}\rangle\langle s+\hat{\mu}|n\rangle \\ &= \sum_s \psi_m^\dagger(s)U_\mu(s)\psi_n(s+\hat{\mu}). \end{aligned} \tag{2.11}$$

This quantity is gauge invariant for the arbitrary modes $|n\rangle$, and $|m\rangle$. In fact, by the gauge transformation Eq.(2.8), the matrix element is transformed as

$$\begin{aligned}\langle m|\hat{U}_\mu|n\rangle &= \sum_s \psi_m^\dagger(s)U_\mu(s)\psi_n(s+\hat{\mu}) \\ &\to \sum_s \psi_m^\dagger(s)V^\dagger(s)\cdot V(s)U_\mu(s)V^\dagger(s+\hat{\mu})V(s+\hat{\mu})\psi_n(s+\hat{\mu}) \\ &= \sum_s \psi_m^\dagger(s)U_\mu(s)\psi_n(s+\hat{\mu}) = \langle m|\hat{U}_\mu|n\rangle. \end{aligned} \tag{2.12}$$

However, the irrelevant n-dependent phase factor appears. Nevertheless, this phase factor cancels as $\mathrm{e}^{i\varphi_n[V]}\mathrm{e}^{-i\varphi_n[V]} = 1$ in the diagonal element $|n\rangle$ and $\langle n|$. In fact, physical quantities such as the Wilson loop and the Polyakov loop have only the diagonal element [51, 61, 62].

The relation between Polyakov loop and Dirac modes on the temporally odd-number lattice

Then, we analytically derive the relations connecting the Polyakov loop and the Dirac modes. First, we derive the analytical relation for the naive Dirac operator (2.3) on the on the temporally odd-number lattice, where the temporal lattice size is odd number. Then, the relation will be generalized for the even lattice.

First of all, consider products of the link-variable operators which correspond to each path. If the path is a closed loop, the functional trace of the associated products of the link-variable operator is gauge invariant and an observable. However, if the path is not a closed loop, the corresponding

quantity is gauge variant and exactly zero as

$$\begin{aligned}
&\mathrm{Tr}_c(\hat{U}_{\mu_1}\hat{U}_{\mu_2}\cdots\hat{U}_{\mu_N}) = \mathrm{tr}_c\sum_s\langle s|\hat{U}_{\mu_1}\hat{U}_{\mu_2}\cdots\hat{U}_{\mu_N}|s\rangle \\
=&\mathrm{tr}_c\sum_s U_{\mu_1}(s)U_{\mu_2}(s+\hat{\mu}_1)\cdots U_{\mu_N}(s+\sum_{k=1}^{N-1}\hat{\mu}_k)\langle s+\sum_{k=1}^{N}\hat{\mu}_k|s\rangle \\
=&0, \qquad (2.13)
\end{aligned}$$

where $\sum_{k=1}^{N}\hat{\mu}_k \neq 0$ is satisfied for non-closed path and N is the length of the path. This is due to the definition of the link-variable operator Eq.(2.1). Also, this fact is understood from Elitzur's theorem [63] that the vacuum expectation values of gauge-variant operators are zero.

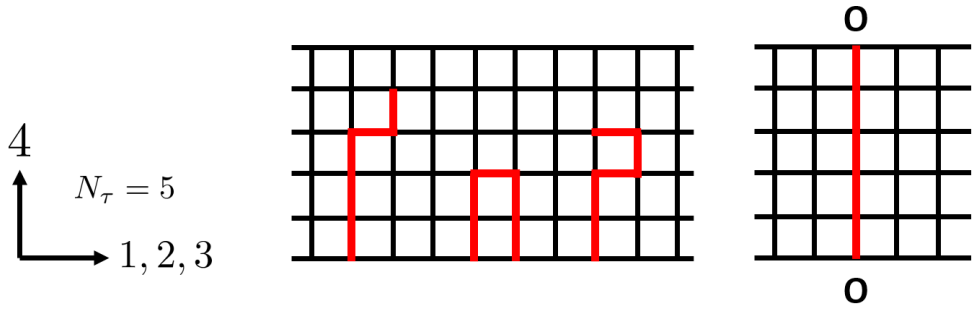

Figure 2.1: An example of odd lattice. This is $N_\tau = 5$ case. Each line corresponds to each term in $\hat{U}_4\hat{\not{D}}^{N_\tau-1}$ in Eq.(2.14). All the lines in the left figure correspond to the gauge-variant terms while the line in the right figure is the unique closed loop using the temporal periodicity, namely the Polyakov loop.

We consider the temporally odd number lattice shown in Fig. 2.1 because the later discussion is very simple and understandable. We use the spatially symmetric lattice, i.e., $N_1 = N_2 = N_3 \equiv N_\sigma$ and $N_4 \equiv N_\tau$, and assume that the spatial length is larger than temporal length. The periodic boundary conditions are imposed on both temporal and spatial directions. These assumptions are not unnatural because the temporal length is finite and the spatial length is infinite in the ideal situation for the continuum theory at finite temperature.

On such a lattice, we introduce a functional trace I defined as

$$I = \mathrm{Tr}_{c,\gamma}(\hat{U}_4\hat{\not{D}}^{N_\tau-1}). \qquad (2.14)$$

Substituting the definition of the Dirac operator (2.3), the functional trace I is expressed as a sum of products of odd-number link-variable operators because N_τ is odd number. Some examples are shown in Fig. 2.1. Note that most of the terms in the expansion of I exactly vanish because one cannot make a closed loop by using odd-number link-variable operators on a square lattice. Thus there is only contribution from the closed path due to the temporal periodicity, that is the Polyakov loop L, which can be closed loop and gauge invariant with odd-number link-variables using the periodic boundary condition. This is why we use the temporally odd-number lattice. In this way, the functional trace I can be expressed as

$$\begin{aligned} I &= \mathrm{Tr}_{c,\gamma}(\hat{U}_4 \hat{\not{D}}^{N_\tau-1}) \\ &= \mathrm{Tr}_{c,\gamma}\{\hat{U}_4(\gamma_4 \hat{D}_4)^{N_\tau-1}\} \\ &= 4\mathrm{Tr}_c(\hat{U}_4 \hat{D}_4^{N_\tau-1}) \\ &= \frac{4}{(2a)^{N_\tau-1}}\mathrm{Tr}_c\{\hat{U}_4(\hat{U}_4 - \hat{U}_{-4})^{N_\tau-1}\} \\ &= \frac{4}{(2a)^{N_\tau-1}}\mathrm{Tr}_c\{\hat{U}_4^{N_\tau}\} \\ &= -\frac{12V}{(2a)^{N_\tau-1}}L. \end{aligned} \tag{2.15}$$

On the other hand, using the completeness of the Dirac mode, the functional trace is expressed as

$$I = \sum_n \langle n|\hat{U}_4\, \hat{\not{D}}^{N_\tau-1}|n\rangle = i^{N_\tau-1}\sum_n \lambda_n^{N_\tau-1}\langle n|\hat{U}_4|n\rangle. \tag{2.16}$$

Therefore, combining Eqs. (2.15) and (2.16), we find a relation

$$L = -\frac{(2ai)^{N_\tau-1}}{12V}\sum_n \lambda_n^{N_\tau-1}\langle n|\hat{U}_4|n\rangle. \tag{2.17}$$

This is a relation directly connecting the Polyakov loop and the Dirac modes, i.e., a Dirac spectral representation of the Polyakov loop.

Note that Eq. (2.17) is gauge invariant relation because the Polyakov loop is gauge invariant quantity and the Dirac modes can be gauge-covariantly calculated. Thus our discussion perfectly respects the gauge symmetry. The relation holds for each gauge configuration, namely an arbitrary set of the link-variables. Consequently, this relation is satisfied regardless of whether the gauge-configuration is generated in full QCD or quenched QCD. However, the Dirac modes, λ_n and $|n\rangle$, are calculated by use of the naive Dirac

operator (2.3). This point is generalized in the later section. Of course, the configuration average of the formula (2.17) is valid.

$$\langle L \rangle = -\frac{(2ai)^{N_\tau - 1}}{12V} \left\langle \sum_n \lambda_n^{N_\tau - 1} \langle n | \hat{U}_4 | n \rangle \right\rangle . \tag{2.18}$$

The outmost bracket $\langle\rangle$ means gauge-configuration average.

From the analytical relation (2.17), the relation between confinement and chiral symmetry breaking in QCD because the Polyakov loop is an order parameter for quark-confinement and the Dirac modes are strongly related with the chiral symmetry breaking via the Banks-Casher relation (1.26). First, we note that the Dirac matrix element is finite: $|\langle n|\hat{U}_4|n\rangle| < 1$. Thus, we can find that the factor $\lambda_n^{N_\tau - 1}$ determines the magnitude of the contribution from each Dirac mode $\lambda_n^{N_\tau - 1}\langle n|\hat{U}_4|n\rangle$. The overall factor is not related with the comparison of the magnitude of each contribution. However, when the Dirac eigenvalue is small $|\lambda_n| \simeq 0$, the factor $\lambda_n^{N_\tau - 1}$ plays as the damping factor. Thus, the contributions from the low-lying Dirac modes are strongly suppressed compared to the other Dirac-mode contribution. However, as discussed in the previous sections, the low-lying Dirac modes are essential modes for the chiral symmetry breaking. Thus, the negligible contribution from the low-lying Dirac modes to the Polyakov loop indicates that the important modes for the chiral symmetry breaking are not important for quark-confinement in QCD. In other words, our analytical discussion suggests that there are no direct one-to-one correspondence between quark-confinement and chiral symmetry breaking in QCD.

In order to derive the relation (2.17), we assume only the following conditions:

1. odd N_τ
2. square lattice
3. temporal periodicity for link-variables

Due to the first assumption, the analytical relation (2.17) is satisfied only on the temporally odd-number lattice. However, this constraint is not so serious because this choice of the parity for the lattice size does not alter the physics in the continuum limit with any large number of N_τ. In fact, the relation (2.17) can be generalized for the even lattice with even N_τ. By the same reason, the second assumption is also not problem. The third assumption is necessary for the finite-temperature formalism. Therefore, the relation (2.17) is fully general and valid in full QCD and in finite temperature and density,

and furthermore regardless of the phase of the system. In other words, the relation holds in confinement and deconfinement phases, and in chiral broken and restored phases.

One might consider that the Polyakov loop and the Dirac modes are not related each other because the Polyakov loop is defined by gauge fields alone and the Dirac modes look are fermionic modes. However, the Polyakov loop in influenced by the quarks, and the Dirac modes are strongly affected by the gauge fields because the Dirac eigenvalue equation (2.7) includes the link-variables. A similar example is instantons. The instantons are defined by gauge fields alone, however they have a close connection to the axial U(1) anomaly, which relates to a fermionic symmetry. Thus, it is not unnatural that the Polyakov loop has a connection to the Dirac modes. Thus, when the dynamical quarks are considered, its effect changes the values of the Polyakov loop L, the Dirac eigenvalue distribution $\rho(\lambda)$ and the matrix elements $\langle n|\hat{U}_\mu|m\rangle$. However, the relation Eq.(2.17) holds even if considering the dynamical quarks.

The relation between Polyakov loop and Dirac modes on the even lattice

Moreover, the Polyakov loop can be expressed in terms of the Dirac modes on the even lattice where all the lattice sizes are even number with the periodic boundary condition for link-variables [61]. It is also derived in the following.

Corresponding to I in Eq.(2.14), we introduce a quantity

$$\tilde{I}(N_\tau) \equiv \mathrm{Tr}_{c,\gamma}(\gamma_4^{\xi(N_\tau)} \hat{U}_4^{N_\tau/2+1} \hat{\not{D}}^{N_\tau/2-1}) \tag{2.19}$$

with $\xi(N_\tau)$ is defined as

$$\xi(N_\tau) = \begin{cases} 0 & (N_\tau/2 : \text{odd}) \\ 1 & (N_\tau/2 : \text{even}) \end{cases} \tag{2.20}$$

This quantity $\hat{U}_4^{N_\tau/2+1} \hat{\not{D}}^{N_\tau/2-1}$ can be expanded as a sum of products of N_τ link-variable operators. An example for the even lattice is shown in Fig. 2.2 and each line corresponds with each term in the expansion of $\hat{U}_4^{N_\tau/2+1} \hat{\not{D}}^{N_\tau/2-1}$ in Eq.(2.19). In $\hat{U}_4^{N_\tau/2+1} \hat{\not{D}}^{N_\tau/2-1}$, any spatially closed loops cannot be made because the number of $\hat{U}_4$ is larger than that of $\hat{U}_{-4}$. Then, $\hat{U}_4^{N_\tau/2+1} \hat{\not{D}}^{N_\tau/2-1}$ does not have any gauge-invariant quantities except for the Polyakov loop, which is the temporally closed loop. Therefore using the temporal periodic

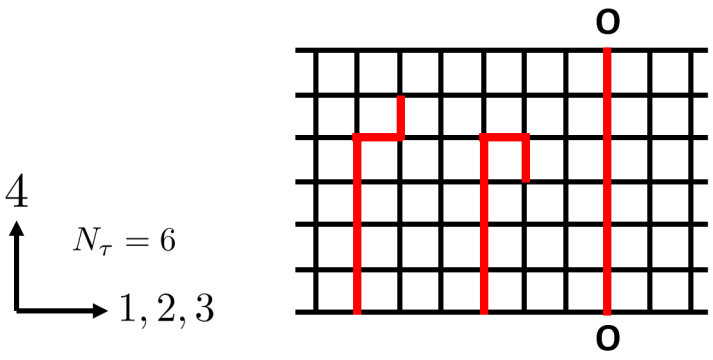

Figure 2.2: An example of even lattice. This is $N_\tau = 6$ case. Each line corresponds to each term in $\hat{U}_4^{N_\tau/2+1}\hat{\not{D}}^{N_\tau/2-1}$ in Eq.(2.19). The Polyakov loop is the unique closed loop using the temporal periodicity.

boundary condition, one finds

$$\begin{aligned}
\tilde{I} &= \mathrm{Tr}_{c,\gamma}(\gamma_4^{\xi(N_\tau)}\hat{U}_4^{N_\tau/2+1}\hat{\not{D}}^{N_\tau/2-1}) \\
&= \mathrm{Tr}_{c,\gamma}\{\gamma_4^{\xi(N_\tau)}\hat{U}_4^{N_\tau/2+1}(\gamma_4\hat{D}_4)^{N_\tau/2-1}\} \\
&= \mathrm{Tr}_{c,\gamma}(\gamma_4^{\xi(N_\tau)+N_\tau/2-1}\hat{U}_4^{N_\tau/2+1}\hat{D}_4^{N_\tau/2-1}) \\
&= 4\mathrm{Tr}_c(\hat{U}_4^{N_\tau/2+1}\hat{D}_4^{N_\tau/2-1}) \\
&= \frac{4}{(2a)^{N_\tau/2-1}}\mathrm{Tr}_c\{\hat{U}_4^{N_\tau/2+1}(\hat{U}_4 - \hat{U}_{-4})^{N_\tau/2-1}\} \\
&= \frac{4}{(2a)^{N_\tau/2-1}}\mathrm{Tr}_c\{\hat{U}_4^{N_\tau}\} \\
&= \frac{12V}{(2a)^{N_\tau/2-1}}L. \qquad (2.21)
\end{aligned}$$

On the other hand, taking Dirac modes as the basis for the functional trace in Eq.(2.19), the quantity $\tilde{I}$ is expressed as

$$\begin{aligned}
\tilde{I} &= \sum_n \langle n|\gamma_4^{\xi(N_\tau)}\hat{U}_4^{N_\tau/2+1}\ \hat{\not{D}}^{N_\tau/2-1}|n\rangle \\
&= i^{N_\tau/2-1}\sum_n \lambda_n^{N_\tau/2-1}\langle n|\gamma_4^{\xi(N_\tau)}\hat{U}_4^{N_\tau/2+1}|n\rangle. \qquad (2.22)
\end{aligned}$$

Combining Eqs.(2.21) and (2.22), the relation is found as

$$L = \frac{(2ai)^{N_\tau/2-1}}{12V}\sum_n \lambda_n^{N_\tau/2-1}\langle n|\gamma_4^{\xi(N_\tau)}\hat{U}_4^{N_\tau/2+1}|n\rangle. \qquad (2.23)$$

In this way, we derive the relation connecting the Polyakov loop L and the Dirac eigenvalues $i\lambda_n$ on the even lattice. Comparing Eqs.(2.17) and (2.23), the form of Eq.(2.17) is simpler than that of Eq.(2.23). However, both equations give the same content of physics because it should be independent of the temporal lattice size N_τ. The dumping factor $\lambda_n^{N_\tau/2-1}$ in RHS of Eq.(2.23) and $\lambda_n^{N_\tau-1}$ in RHS of Eq.(2.17) are expected to have the same roles.

As we discuss in the previous section, the analytical relations Eqs. (2.17) and (2.23) indicate small contribution from low-lying Dirac modes to the Polyakov loop. However, it is also important to quantitatively confirm the expectation. For simplicity, we consider the temporally odd-number lattice, namely Eq. (2.17).

Since Eq. (2.17) is given as a sum over all the Dirac modes, each term expresses the individual contribution from each Dirac mode and it can be numerically obtained for the quantitative discussion. In the relation (2.17), the Dirac matrix element $\langle n|\hat{U}_\mu|m\rangle$ can be explicitly written as Eq.(2.11). Thus, the relation (2.17) is expressed as

$$L = -\frac{(2ai)^{N_\tau-1}}{12V}\sum_n \lambda_n^{N_\tau-1}\sum_s \psi_n^\dagger(s)U_4(s)\psi_n(s+\hat{4}). \tag{2.24}$$

In principle, the Dirac eigenvalues λ_n and the Dirac eigenfunctions $\psi_n(s)$ in RHS of Eq. (2.24) can be obtained by solving the Dirac eigenequation (2.7) for each gauge configuration generated in the Monte-Carlo simulation. However, it is not easy task because the numerical cost for solving the Dirac eigenequation is very large. In fact, the dimension of the Dirac operator $(4 \times N_{\rm c} \times V)^2$, it is very huge in general. Nevertheless, using the Kogut-Susskind (KS) formalism [64], the numerical cost can be partially reduced without approximation. We discuss it in the next part.

Modified Kogut-Susskind formalism for temporally odd-number lattice

All the eigenvalues and the eigenmodes of the Dirac operator $\not{D}$ defined by Eq.(2.3) are needed for the quantitative analysis for the relation between confinement and chiral symmetry breaking in QCD. In order to reduce the numerical cost, the technique of the KS formalism for diagonalizing the Dirac operator $\not{D}$ is useful. The KS formalism is originally given by Kogut and Susskind [64]. However, it is applicable to only the even lattice, where all the lattice sizes are even number with the periodic boundary condition. Hence, it is not applicable to the temporally odd-number lattice. However, the KS

formalism have been generalized for the temporally odd-number lattice in our study [61]. In the following, we discuss "modified KS formalism" on the temporally odd-number lattice after we review the KS formalism on the even lattice.

The KS formalism is the method for spin-diagonalizing the naive Dirac operator on the lattice. We consider the even lattice, where all the lattice sizes $N_{1\sim4}$ are even numbers. A matrix $T(s)$ is defined as

$$T(s) \equiv \gamma_1^{s_1}\gamma_2^{s_2}\gamma_3^{s_3}\gamma_4^{s_4}. \tag{2.25}$$

This matrix depends on all the components of the site $s = (s_1, s_2, s_3, s_4)$. Using the matrix, one can diagonalize all the γ-matrices γ_μ ($\mu = 1, 2, 3, 4$);

$$T^\dagger(s)\gamma_\mu T(s \pm \hat{\mu}) = \eta_\mu(s)\mathbf{1}, \tag{2.26}$$

where the staggered phase $\eta_\mu(s)$ is introduced as

$$\eta_1(s) \equiv 1, \quad \eta_\mu(s) \equiv (-1)^{s_1+\cdots+s_{\mu-1}} \ (\mu \geq 2). \tag{2.27}$$

Note that the Dirac operator $\not{D} = \gamma_\mu D_\mu$ is linear in the γ-matrices. Thus, the Dirac operator is spin-diagonalized as

$$\begin{aligned}\sum_\mu T^\dagger(s)\gamma_\mu D_\mu T(s+\hat{\mu}) \\ = \mathrm{diag}(\eta_\mu D_\mu, \eta_\mu D_\mu, \eta_\mu D_\mu, \eta_\mu D_\mu),\end{aligned} \tag{2.28}$$

where the KS Dirac operator $\eta_\mu D_\mu$ is defined as

$$(\eta_\mu D_\mu)_{ss'} = \frac{1}{2a}\sum_{\mu=1}^{4}\eta_\mu(s)\left[U_\mu(s)\delta_{s+\hat{\mu},s'} - U_{-\mu}(s)\delta_{s-\hat{\mu},s'}\right]. \tag{2.29}$$

From the Eq. (2.28), one can find fourfold degeneracy of the Dirac eigenvalue $i\lambda_n$ relating to the spinor structure of the Dirac operator. Thus, all the eigenvalues of the Dirac operator can be obtained by only solving the KS Dirac eigenvalue equation

$$\eta_\mu D_\mu |n) = i\lambda_n |n) \tag{2.30}$$

where $|n)$ is the KS Dirac eigenstate. Note that the KS Dirac operator has only indices of sites and colors, not spinors. Thus, the numerical cost for solving the KS Dirac eigenvalue equation (2.30) is smaller than that for the Dirac eigenvalue equation (2.7), and the ratio is about 1/16. Using the KS

Dirac eigenfunction $\chi_n(s) \equiv \langle s|n)$, the KS Dirac eigenvalue equation (2.30) is explicitly expressed as

$$\frac{1}{2a}\sum_{\mu=1}^{4}\eta_\mu(s)[U_\mu(s)\chi_n(s+\hat{\mu}) - U_{-\mu}(s)\chi_n(s-\hat{\mu})] = i\lambda_n\chi_n(s). \tag{2.31}$$

Also, KS Dirac matrix element $(n|\hat{U}_\mu|m)$ is expressed as

$$\begin{aligned}(n|\hat{U}_\mu|m) &= \sum_s (n|s\rangle\langle s|\hat{U}_\mu|s+\hat{\mu}\rangle\langle s+\hat{\mu}|m) \\ &= \sum_s \chi_n(s)^\dagger U_\mu(s)\chi_m(s+\hat{\mu}).\end{aligned} \tag{2.32}$$

Because of fourfold degeneracy of the Dirac eigenvalue, there are four states with the same eigenvalues. These states are labeled with quantum number $I = 1, 2, 3, 4$, namely $|n, I\rangle$ [12]. Using this notation, the Dirac eigenvalue equation (2.7) can be expressed as

$$\not{D}|n, I\rangle = i\lambda_n|n, I\rangle. \tag{2.33}$$

The relation between the Dirac eigenfunction $\psi_n^I(s)_\alpha \equiv \langle s, \alpha|n, I\rangle$ and the spinless KS-Dirac eigenfunction $\chi_n(s)$ is

$$\psi_n^I(s)_\alpha = T(s)_{\alpha I}\chi_n(s). \tag{2.34}$$

The quantum number I is mixed with spinor indices. That can be understood from the fact that the quantum number I comes from the fourfold degeneracy of the Dirac eigenvalue in the spinor space.

At the temporal boundary, the matrix satisfies

$$T(s + N_\tau\hat{4}) = T(s)\gamma_4^{N_\tau}. \tag{2.35}$$

Then, the matrix $T(s)$ is periodic if the temporal length N_τ is even number. Since this situation holds in all the directions, the periodic boundary condition

$$T(s + N_\mu\hat{\mu}) = T(s) \tag{2.36}$$

is satisfied only on the even lattice. Although the spatial periodic boundary condition is not necessarily need physically, the temporal periodic boundary condition is necessary for the imaginary-time finite-temperature formalism.

Therefore, the original KS formalism is not applicable to the temporally odd-number lattice.

Note here that this procedure is just a mathematical technique to diagonalize $\not{D}$, and this never means to use a specific fermion like the KS fermion. In fact, the diagonalization of $\not{D}$ is mathematically equivalent to the use of the KS formalism.

Now, we present the modified KS formalism as the generalization applicable to the temporally odd-number lattice, where the lattice size for temporal direction N_τ is odd number and the lattice sizes for spatial direction N_i $(i = 1, 2, 3)$ are even number with the periodic boundary conditions for all the directions.

Instead of the matrix $T(s)$, a matrix $M(s)$ is introduced by

$$M(s) \equiv \gamma_1^{s_1}\gamma_2^{s_2}\gamma_3^{s_3}\gamma_4^{s_1+s_2+s_3}. \tag{2.37}$$

Although the matrix $M(s)$ is similar to the matrix $T(s)$, it is independent of the time component of the site s_4. Using the matrix $M(s)$, all the $\gamma-$matrices are transformed to be proportional to γ_4:

$$M^\dagger(s)\gamma_\mu M(s \pm \hat{\mu}) = \eta_\mu(s)\gamma_4, \tag{2.38}$$

where $\eta_\mu(s)$ is the staggered phase given by Eq. (2.27). This relation 2.38 is always satisfied for arbitrary representation for the gamma matrices. In the Dirac representation, γ_4 is diagonal as

$$\gamma_4 = \begin{pmatrix} 1 & 0 & 0 & 0 \\ 0 & 1 & 0 & 0 \\ 0 & 0 & -1 & 0 \\ 0 & 0 & 0 & -1 \end{pmatrix} \tag{2.39}$$

and the Dirac representation is taken in this paper. Thus, the Dirac operator $\not{D} = \gamma_\mu D_\mu$ can be spin-diagonalized also on the temporally odd-number lattice:

$$\sum_\mu M^\dagger(s)\gamma_\mu D_\mu M(s+\hat{\mu}) = \begin{pmatrix} \eta_\mu D_\mu & 0 & 0 & 0 \\ 0 & \eta_\mu D_\mu & 0 & 0 \\ 0 & 0 & -\eta_\mu D_\mu & 0 \\ 0 & 0 & 0 & -\eta_\mu D_\mu \end{pmatrix}, \tag{2.40}$$

where $\eta_\mu D_\mu$ is the KS Dirac operator given in Eq. (2.29).

Note that the modified KS formalism can be applicable to the temporally odd-number lattice. because the periodic boundary condition for the matrix $M(s)$ is satisfied for any direction. In fact, at the temporal boundary,

$$M(s + N_4\hat{4}) = M(s), \tag{2.41}$$

is trivially satisfied because $M(s)$ is independent of s_4. Moreover, the spatial boundary conditions for each direction

$$M(s + N_i\hat{i}) = M(s) \qquad (i = 1, 2, 3) \tag{2.42}$$

is valid because the spatial lattice sizes are even number. The staggered phase $\eta_\mu(s)$ satisfies the periodic boundary condition on the temporally odd-number lattice because the staggered phase $\eta_\mu(s)$ is also independent of the time component of the site s_4. In this way, the KS formalism can be generalized for the temporally odd-number lattice.

The Dirac operator has two positive modes and two negative modes for each eigenvalue λ_n on the temporally odd-number lattice from Eq. (2.40). From the anti-commutator relation (1.14), the existence of the chiral partner $\gamma_5|n\rangle$ is guaranteed with the eigenvalue $-i\lambda_n$. Thus, also on the temporally odd-number lattice, all the eigenvalues of the Dirac operator can be obtained only by solving the KS Dirac eigenvalue equation (2.31).

In the case of the temporally odd-number lattice, the Dirac eigenstates are labeled with quantum number $I = 1, 2, 3, 4$ according to the spinor structure of the Dirac operator given by Eq. (2.40). These four Dirac eigenfunction $\psi_n^I(s)_\alpha \equiv \langle s, \alpha|n, I\rangle$ are constructed For each KS Dirac mode $|n)$ as

$$\psi_n^I(s)_\alpha = M(s)_{\alpha I}\chi_n(s). \tag{2.43}$$

The Dirac eigenstates $|n, I\rangle$ have the eigenvalue $i\lambda_n$ with $I = 1, 2$ and have the eigenvalue $-i\lambda_n$ with $I = 3, 4$.

Next, the relation (2.17) is rewritten using the KS Dirac modes. Now the relation (2.17) is correctly written as

$$L = -\frac{(2ai)^{N_\tau - 1}}{12V}\sum_{n,I}\lambda_n^{N_\tau - 1}\langle n, I|\hat{U}_4|n, I\rangle. \tag{2.44}$$

The diagonal Dirac matrix element $\langle n, I|\hat{U}_4|n, I\rangle$ can be expressed by the diagonal KS Dirac matrix element $(n|\hat{U}_4|n)$:

$$\langle n, I|\hat{U}_4|n, I\rangle = (n|\hat{U}_4|n). \tag{2.45}$$

The detailed derivation is shown in Appendix A.2). Using the relation (2.45), and taking the structure of the Dirac eigenfunction (2.43) into consideration.

RHS of Eq. (2.44) can be rewritten using the KS Dirac modes:

$$\begin{aligned}
&\sum_{n,I} \lambda_n^{N_4-1} \langle n, I|\hat{U}_4|n, I\rangle \\
&\quad = \sum_{n,I=1,2} \lambda_n^{N_4-1} \langle n, I|\hat{U}_4|n, I\rangle \\
&\qquad + \sum_{n,I=3,4} (-\lambda_n)^{N_4-1} \langle n, I|\hat{U}_4|n, I\rangle \\
&\quad = \sum_{n,I=1,2,3,4} \lambda_n^{N_4-1} \langle n, I|\hat{U}_4|n, I\rangle \\
&\quad = \sum_{n,I=1,2,3,4} \lambda_n^{N_4-1} (n|\hat{U}_4|n) \\
&\quad = 4 \sum_{n} \lambda_n^{N_4-1} (n|\hat{U}_4|n),
\end{aligned} \tag{2.46}$$

where $N_4 - 1$ is even number on the temporally odd-number lattice. Thus, the relation (2.17) is rewritten as

$$L = -\frac{(2ai)^{N_\tau-1}}{3V} \sum_{n} \lambda_n^{N_\tau-1} (n|\hat{U}_4|n) \tag{2.47}$$

using the modified KS formalism. Note that the (modified) KS formalism is an exact mathematical method for spin-diagonalizing the Dirac operator, not an approximation. Thus Eqs. (2.44) and (2.47) are exactly equivalent. Therefore, each Dirac-mode contribution to the Polyakov loop can be obtained by solving the eigenvalue equation of the KS Dirac operator whose dimension is $(N_c \times V)^2$ instead of the original Dirac operator whose dimension is $(4 \times N_c \times V)^2$ on the temporally odd-number lattice.

Note again that a specific fermion like the KS fermion is not used. We just use the KS formalism for diagonalizing the naive Dirac operator $\not{D}$ defined by Eq.(2.3), and obtain all the eigenvalues and the eigenfunctions. Actually, all the eigenvalues and eigenfunctions can be obtained without the KS formalism by the direct diagonalization of the Dirac operator $\not{D}$, and they gives the same results. however, the numerical cost is larger.

Numerical analysis

Next, the numerical analysis is shown for the relation between confinement and chiral symmetry breaking in QCD based on the relation (2.47) connecting the Polyakov loop and Dirac modes on the temporally-odd number lattice.

The eigenvalue and engenfunction of the KS Dirac operator is obtained by using the Linear Algebra PACKage (LAPACK) [65].

The SU(3) lattice QCD Monte Carlo simulations are performed at the quenched level with the standard Wilson plaquette action in both cases of confinement and deconfinement phases. The lattice setup is $10^3 \times 5$ with $\beta \equiv \frac{2N_c}{g^2} = 5.6$ (i.e., $a \simeq 0.25$ fm), and $10^3 \times 3$ with $\beta = 5.7$ (i.e., $a \simeq 0.20$ fm), The former corresponds to $T \equiv 1/(N_\tau a) \simeq 160$ MeV, and it describes the confinement phase. The latter corresponds to $T \equiv 1/(N_\tau a) \simeq 330$ MeV, and it describes the deconfinement phase. 20 gauge configurations are used for each phase, and they are taken every 500 sweeps after the thermalization of 5,000 sweeps.

In order to confirm that the relation (2.47) is satisfied numerically, we have independently calculated LHS and RHS of the relation (2.47) and compare them. The numerical results for each gauge-configuration in both confinement and deconfinement phases are shown in Table 2.1 and Table 2.2, respectively.

Table 2.1: Numerical results for LHS and RHS of the relation (2.47) on the $10^3 \times 5$ lattice with $\beta = 5.6$ for each gauge configuration, where the system is in confinement phase. L_D is defined as the R.H.S of the relation (2.47). This table is essentially same as that in Ref. [61].

configuration No.	ReL	ImL	Re$L_{\rm D}$	Im$L_{\rm D}$
1	0.00961	-0.00322	0.00961	-0.00322
2	-0.00161	-0.00125	-0.00161	-0.00125
3	0.0139	-0.00438	0.0139	-0.00438
4	-0.00324	-0.00519	-0.00324	-0.00519
5	0.000689	-0.0101	0.000689	-0.0101
6	0.00423	-0.0168	-0.00423	-0.0168
7	-0.00807	-0.00265	-0.00807	-0.00265
8	-0.00918	-0.00683	-0.00918	-0.00683
9	0.00624	-0.00448	0.00624	-0.00448
10	-0.00437	0.00700	-0.00437	0.00700

From Tables 2.1 and 2.2, it is found that Eq. (2.47) is exactly valid for each gauge configuration in both confinement and deconfinement phases as expected above. In fact, the Elitzur's theorem is not necessary for the derivation of the relation because it is satisfied for each gauge-configuration. Then, we can quantitatively investigate the relation between confinement and chiral symmetry breaking in QCD using the relation (2.47) with a single gauge-configuration.

Table 2.2: Numerical results for LHS and RHS of the relation (2.47) on the $10^3 \times 3$ lattice with $\beta = 5.7$ for each gauge configuration, where the system is in deconfinement phase. This table is essentially same as that in Ref. [61].

configuration No.	ReL	ImL	Re$L_{\rm D}$	Im$L_{\rm D}$
1	0.316	-0.00104	0.316	-0.00104
2	0.337	-0.00597	0.337	-0.00597
3	0.331	0.00723	0.331	0.00723
4	0.305	-0.00334	0.305	-0.00334
5	0.313	0.00167	0.314	0.00167
6	0.316	0.000120	0.316	0.000120
7	0.337	0.000482	0.337	0.000482
8	0.300	-0.00690	0.300	-0.00690
9	0.344	-0.00102	0.344	-0.00102
10	0.347	-0.00255	0.347	-0.00255

In the deconfinement phase, the Z_3 center symmetry at the quenched level is spontaneously broken, and the Polyakov loop is proportional to $\mathrm{e}^{i\frac{2\pi}{3}k}$ ($k = 0, \pm 1$) for each gauge configuration [12]. In this paper, the vacuum where the Polyakov loop is almost real (j=0) is referred to as the "real Polyakov-loop vacuum" and the other vacua is called as the "Z_3-rotated vacua." At the quenched level, it is numerically confirmed that the relation (2.47) is exactly satisfied in the Z_3-rotated vacua as well as the real Polyakov-loop vacuum.

In the case of the full QCD calculations, where dynamical quarks are included, the real Polyakov-loop vacuum is selected as the stable vacuum, and the Z_3-rotated vacua are meta-stable states. Then, the real Polyakov-loop vacuum would be more significant than other vacua in the deconfinement phase. Even in full QCD, the mathematical relation (2.47) is exact because it is not related to how the link-variables are generated.

Next, we numerically investigate each Dirac-mode contribution in order to confirm that the low-lying Dirac modes have negligible contribution to the Polyakov loop based on the relation (2.47). This is expected from the analytical relation (2.47) as discussed above, however, the quantitative numerical analysis is also meaningful.

Since RHS of the Eq. (2.47) is expressed as a sum over the Dirac-mode contribution, the individual contribution to the Polyakov loop from each Dirac mode. Then, the Polyakov loop without low-lying Dirac-mode contri-

bution is introduced as

$$L_{\text{IR-cut}} = -\frac{(2ai)^{N_\tau-1}}{3V}\sum_{|\lambda_n|>\Lambda_{\text{IR}}}\lambda_n^{N_\tau-1}(n|\hat{U}_4|n), \tag{2.48}$$

where Λ_{IR} is the infrared (IR) cutoff for Dirac eigenvalue λ_n. The chiral condensate $\langle\bar{q}q\rangle$ is expressed on the lattice as

$$\begin{aligned}\langle\bar{q}q\rangle &= -\frac{1}{V}\text{Tr}_{c,\gamma}\frac{1}{\not{D}+m} \\ &= -\frac{1}{V}\sum_n\frac{1}{i\lambda_n+m} \\ &= -\frac{1}{V}\left(\sum_{\lambda_n>0}\frac{2m}{\lambda_n^2+m^2}+\frac{\nu}{m}\right),\end{aligned} \tag{2.49}$$

where m is the current quark mass and ν the total number of zero modes of $\not{D}$.

In Fig. 2.3, the Dirac eigenvalue distribution $\rho(\lambda)$ in confinement and deconfinement phases are shown. In the deconfinement phase, the density of low-lying Dirac-modes is small and $\rho(\lambda=0)\simeq 0$. It means that the chiral condensate is almost zero and the chiral symmetry is restored. Then, in the deconfinement phase, the effect of low-lying Dirac-modes to the Polyakov loop might not be interesting because low-lying Dirac-modes are almost absent.

After the removal of contribution from the low-lying Dirac modes below IR cutoff Λ_{IR}, the chiral condensate is written as

$$\langle\bar{q}q\rangle_{\Lambda_{\text{IR}}} = -\frac{1}{V}\sum_{\lambda_n\geq\Lambda_{\text{IR}}}\frac{2m}{\lambda_n^2+m^2} \tag{2.50}$$

In this thesis, the IR cutoff is set as $\Lambda_{\text{IR}}\simeq 0.4$GeV. In the confined phase, using this IR Dirac-mode cut, chiral-symmetry is almost restored, and the chiral condensate is strongly reduced as

$$\frac{\langle\bar{q}q\rangle_{\Lambda_{\text{IR}}}}{\langle\bar{q}q\rangle}\simeq 0.02 \tag{2.51}$$

in the case of physical current-quark mass, $m\simeq 5$MeV [51].

For 10 gauge configurations, the numerical results for L and $L_{\text{IR-cut}}$ in both confinement and deconfinement phases are shown in Tables 2.3 and 2.4, respectively.

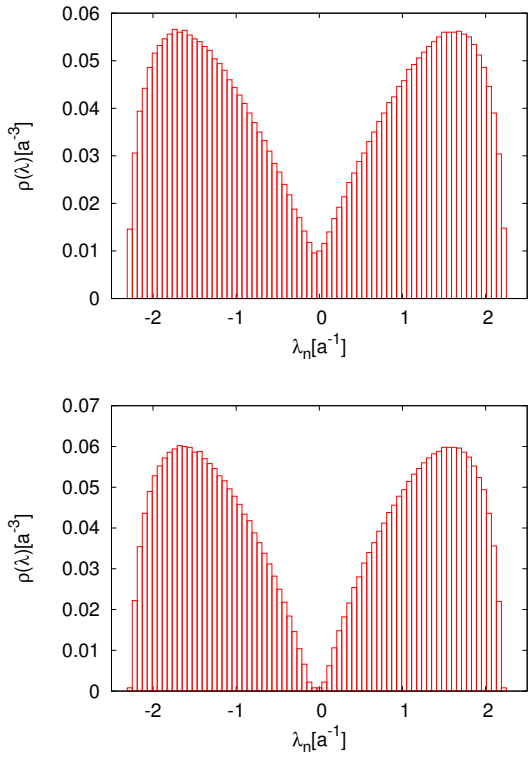

Figure 2.3: The lattice QCD result for the Dirac eigenvalue distribution $\rho(\lambda)$ in confinement and deconfinement phases in the lattice unit. The upper figure is the results on $10^3 \times 5$ lattice with $\beta = 5.6$ (i.e., $a \simeq 0.25$ fm), where the system is in the confinement phase. The lower figure is the results on $10^3 \times 5$ lattice with $\beta = 6.0$ (i.e., $a \simeq 0.10$ fm). where the system is in the deconfinement phase. These figures are taken from Ref. [61].

From Tables 2.3 and 2.4, it is found that

$$L \simeq L_{\text{IR-cut}} \tag{2.52}$$

is almost satisfied for each gauge configuration in both confinement and deconfinement phases. In the deconfinement phase, we have confirmed that $L \simeq L_{\text{IR-cut}}$ is valid for both real Polyakov-loop vacuum and Z_3-rotated vacua. Thus, the configuration average $\langle L \rangle \simeq \langle L_{\text{IR-cut}} \rangle$ is of course almost satisfied. Therefore, the low-lying Dirac modes have negligible contribution to the Polyakov loop. This results suggest that the low-lying Dirac modes below the IR cutoff $|\lambda_n| < \Lambda_{\text{IR}} \simeq 0.4$GeV are not essential for confinement while they are essential for chiral symmetry breaking From Eq. (2.51). Thus,

Table 2.3: Numerical results for L and $L_{\text{IR-cut}}$ on the $10^3 \times 5$ lattice with $\beta = 5.6$ for each gauge configuration, where the system is in confinement phase. This table is essentially same as that in Ref. [61].

configuration No.	ReL	ImL	Re$L_{\text{IR-cut}}$	Im$L_{\text{IR-cut}}$
1	0.00961	-0.00322	0.00961	-0.00321
2	-0.00161	-0.00125	-0.00160	-0.00125
3	0.0139	-0.00438	0.0139	-0.00437
4	-0.00324	-0.00519	-0.00325	-0.00520
5	0.000689	-0.0101	0.000706	-0.0101
6	0.00423	-0.0168	0.00422	-0.0168
7	-0.00807	-0.00265	-0.00807	-0.00264
8	-0.00918	-0.00683	-0.00918	-0.00682
9	0.00624	-0.00448	0.00624	-0.00448
10	-0.00437	0.00700	-0.00436	0.00698

our results indicate that there is no direct one-to-one correspondence between confinement and chiral symmetry breaking in QCD.

New "positive/negative symmetry" on Dirac matrix element in confinement phase

We investigate the properties of the matrix element $(n|\hat{U}_4|n)$ and each Dirac-mode contribution $\lambda_n^{N_\tau-1}(n|\hat{U}_4|n)$ in both confinement and deconfinement phases. The Polyakov loop is obtained by multiplying all the sum of each Dirac-mode contribution $\sum_n \lambda_n^{N_\tau-1}(n|\hat{U}_4|n)$ by the overall factor $-(2ai)^{N_\tau-1}/(3V)$ in Eq. (2.47).

In Fig. 2.4, the numerical results for the matrix elements $\mathrm{Re}(n|\hat{U}_4|n)$ and $\mathrm{Im}(n|\hat{U}_4|n)$ in confinement phase are shown. They are plotted against Dirac eigenvalues λ_n in the lattice unit for one gauge configuration. In Fig. 2.5, each Dirac-mode contribution to the Polyakov loop $\lambda_n^{N_\tau-1}\mathrm{Re}(n|\hat{U}_4|n)$ and $\lambda_n^{N_\tau-1}\mathrm{Im}(n|\hat{U}_4|n)$ are shown in the confinement phase. They are plotted against Dirac eigenvalues λ_n in the lattice unit. From Fig. 2.4, it is found that the real part of the matrix element $\mathrm{Re}(n|\hat{U}_4|n)$ is generally nonzero in the confinement phase, and it is not small in low-lying Dirac-mode region with $|\lambda_n| \sim 0$. However, from Fig. 2.5, it is directly confirmed that the Dirac-mode contribution to the Polyakov loop, $\lambda_n^{N_\tau-1}\mathrm{Re}(n|\hat{U}_4|n)$, is small in low-lying Dirac-mode region thanks to the damping factor $\lambda_n^{N_\tau-1}$ Thus, the damping factor $\lambda_n^{N_\tau-1}$ plays an important role in the Eq. (2.47).

On the other hand, from Fig. 2.4, the imaginary part $\mathrm{Im}(n|\hat{U}_4|n)$ of the

Table 2.4: Numerical results for L and $L_{\text{IR-cut}}$ on the $10^3 \times 3$ lattice with $\beta = 5.7$ for each gauge configuration, where the system is in deconfinement phase. This table is essentially same as that in Ref. [61].

configuration No.	ReL	ImL	Re$L_{\text{IR-cut}}$	Im$L_{\text{IR-cut}}$
1	0.316	-0.00104	0.319	-0.00103
2	0.337	-0.00597	0.340	-0.00597
3	0.331	0.00723	0.334	0.00724
4	0.305	-0.00334	0.307	-0.00333
5	0.314	0.00167	0.317	0.00167
6	0.316	0.000120	0.319	0.000121
7	0.337	0.0000482	0.340	0.0000475
8	0.300	-0.00690	0.303	-0.00691
9	0.344	-0.00102	0.347	-0.00102
10	0.347	-0.00255	0.350	-0.00256

matrix element is relatively small in low-lying Dirac-mode region unlike the case of the real part, $\text{Re}(n|\hat{U}_4|n)$. However, as shown in Fig. 2.5, the low-lying Dirac mode contribution to the imaginary part of the Polyakov loop, $\lambda_n^{N_\tau-1}\text{Im}(n|\hat{U}_4|n)$ is small.

As a remarkable feature, from Fig. 2.4, one can find a new symmetry of "positive/negative symmetry" in the distribution of Dirac-mode matrix element $(n|\hat{U}_4|n)$, namely $\text{Re}(n|\hat{U}_4|n)$ and $\text{Im}(n|\hat{U}_4|n)$ in the confinement phase. Since the damping factor trivially has the same symmetry, the distribution of each Dirac-mode contribution to the Polyakov loop, $\lambda_n^{N_\tau-1}(n|\hat{U}_4|n)$, has the same symmetry. The Polyakov loop is proportional to all the sum of each Dirac-mode contribution to the Polyakov loop, and the zero-value of the Polyakov loop $\langle L \rangle = 0$ comes from the new symmetry in the confinement phase. Moreover, due to the symmetry in the confinement phase, the contribution to the Polyakov loop from arbitrary Dirac-mode region $\Lambda_1 \leq \lambda_n \leq \Lambda_2$ is zero:

$$\sum_{\Lambda_1 \leq \lambda_n \leq \Lambda_2} \lambda_n^{N_\tau-1}(n|\hat{U}_4|n) = 0 \quad \text{(in the confinement phase)}. \tag{2.53}$$

This behavior in the confinement phase is consistent with the previous works [51, 52].

Since quarks are deconfined and the chiral symmetry is restored in the deconfinement phase, it might be less interesting to consider their relation. In the following, only the real Polyakov-loop vacuum is considered because it is selected as the stable vacuum in full QCD.

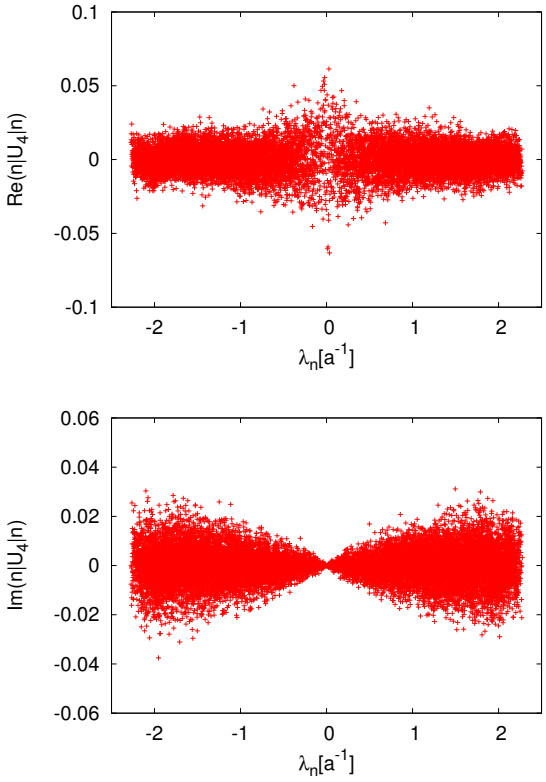

Figure 2.4: The numerical results for the real part $\mathrm{Re}(n|\hat{U}_4|n)$ and the imaginary part $\mathrm{Im}(n|\hat{U}_4|n)$ of the KS-Dirac matrix element in the confinement phase, plotted against the Dirac eigenvalue λ_n in the lattice unit on $10^3 \times 5$ with $\beta = 5.6$. One can find the positive/negative symmetry in the distributions. These figures are taken from Ref. [61].

In Figs. 2.6 and 2.7, the matrix elements $(n|\hat{U}_4|n)$ and each Dirac-mode contribution $\lambda_n^{N_\tau - 1}\mathrm{Re}(n|\hat{U}_4|n)$ in the deconfinement phase with real Polyakov loop. They are plotted against the Dirac eigenvalue λ_n. Since the imaginary part of the Polyakov loop is also zero in the real Polyakov-loop vacuum, the imaginary part $\mathrm{Im}(n|\hat{U}_4|n)$ of the matrix element shows the same behavior as the case of the confinement phase. (Compare Fig. 2.4(b) and Fig. 2.6(b).) Then, only the results for real part of these quantities are considered in the deconfinement phase. The results for a single gauge configuration are shown like the case of the confinement phase because the results show almost same behavior as the other configuration.

From Fig. 2.6, one can find a peak structure in the distribution of the

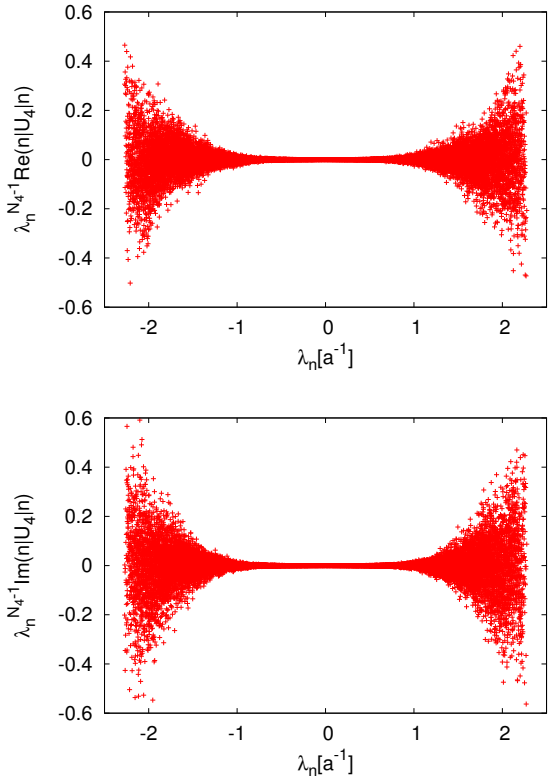

Figure 2.5: The numerical results for each Dirac-mode contribution to the Polyakov loop, $\lambda_n^{N_\tau-1}\mathrm{Re}(n|\hat{U}_4|n)$ and $\lambda_n^{N_\tau-1}\mathrm{Im}(n|\hat{U}_4|n)$ in the confinement phase, plotted against the Dirac eigenvalue λ_n in the lattice unit on $10^3 \times 5$ with $\beta = 5.6$. These figures are taken from Ref. [61].

real part $\mathrm{Re}(n|\hat{U}_4|n)$ of the matrix element in the low-lying mode region. However, like the case of the confinement phase, from Fig. 2.7, each Dirac-mode contribution $\lambda_n^{N_\tau-1}\mathrm{Re}(n|\hat{U}_4|n)$ is relatively small in low-lying Dirac-mode region due to the damping factor $\lambda_n^{N_\tau-1}$. More quantitatively, from Fig. 2.7, since the distribution of the matrix element in the intermediate region is almost symmetric, only the high-lying Dirac modes have nonzero contribution to the Polyakov loop.

In the deconfinement phase, there is no more positive/negative symmetry for the distributions of the matrix element $(n|\hat{U}_4|n)$ and each Dirac-mode contribution $\lambda_n^{N_\tau-1}(n|\hat{U}_4|n)$, unlike the case of the confinement phase with the symmetry. The Polyakov loop is nonzero because of the asymmetry in the distribution of the matrix element and each Dirac-mode contribution, while

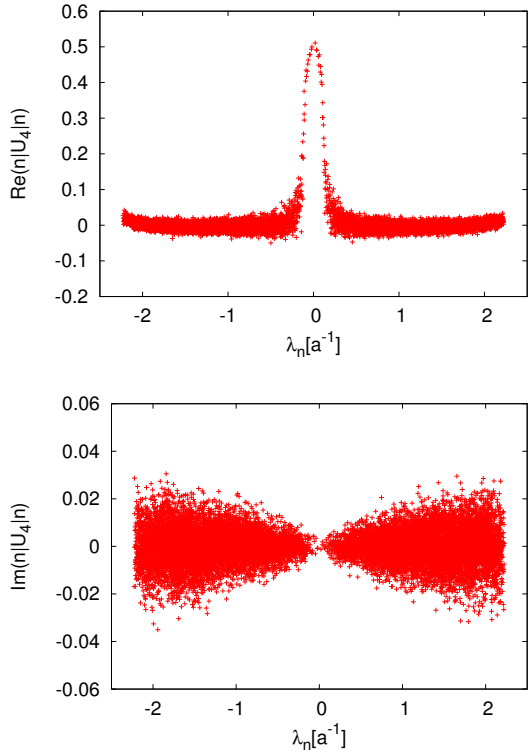

Figure 2.6: The numerical results for the real part $\mathrm{Re}(n|\hat{U}_4|n)$ and the imaginary part $\mathrm{Im}(n|\hat{U}_4|n)$ of the KS-Dirac matrix element in the real Polyakov-loop vacuum in the deconfinement phase, plotted against the Dirac eigenvalue λ_n in the lattice unit on $10^3 \times 3$ with $\beta = 5.7$. there is no positive/negative symmetry in the distribution of the real part $\mathrm{Re}(n|\hat{U}_4|n)$ unlike the confinement phase. These figures are taken from Ref. [61].

the Polyakov loop in the confinement phase is zero because of the symmetry. Thus, the appearance of the positive/negative symmetry on the matrix element $(n|\hat{U}_4|n)$ is strongly related to deconfinement phase transition. This behavior is similar to the Z_3 center symmetry, which is not broken in the confinement phase and is broken in the deconfinement phase at the quenched level. Therefore, it is interesting to investigate the relation between the new positive/negative symmetry and the Z_3 center symmetry.

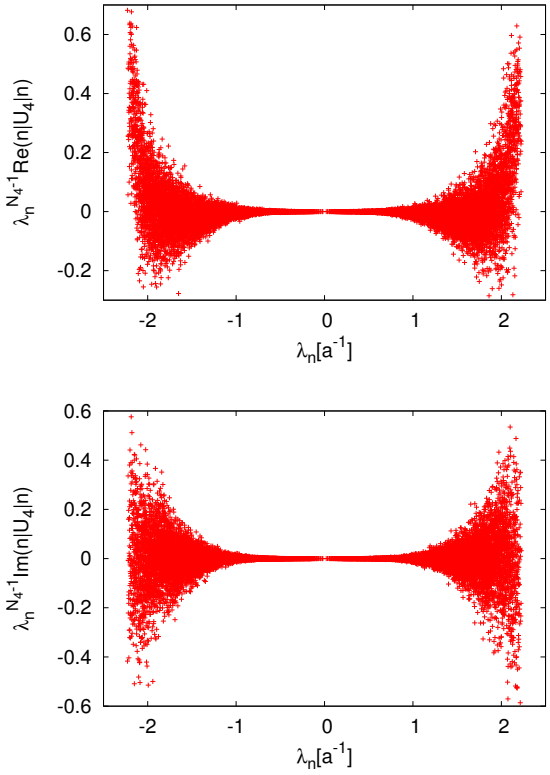

Figure 2.7: The numerical results for each Dirac-mode contribution to the Polyakov loop, $\lambda_n^{N_\tau-1}\mathrm{Re}(n|\hat{U}_4|n)$ and $\lambda_n^{N_\tau-1}\mathrm{Im}(n|\hat{U}_4|n)$, in the real Polyakov-loop vacuum in the deconfinement phase plotted against the Dirac eigenvalue λ_n in the lattice unit on $10^3 \times 3$ with $\beta = 5.7$. These figures are taken from Ref. [61].

2.2 Polyakov loop fluctuations

In this section, we will improve the discussion on the relation between the Polyakov loop and the Dirac modes by considering the Polyakov loop fluctuations [66]. In fact, there are 2 reasons to consider the Polyakov loop fluctuations. One is the correctness of the order parameter for the deconfinement and the other is the ambiguity for the renormalization of the Polyakov loop.

The pure SU(3) gauge theory corresponds to the quenched QCD, quarks are treated as the heavy probes. However, the theory interested is the real QCD where quark masses are small. If the quark is light, the behavior of the Polyakov loop changes due to the explicit breaking of the Z_3 center

symmetry. On the one hand, the Polyakov loop is an exact order parameter of the Z_3 center symmetry and for deconfinement, which leads a first order phase transition in the quenched QCD [12, 67, 68, 69]. On the other hand, in the presence of light dynamical quarks, the Polyakov loop is no longer an order parameter for the deconfinement transition and is smoothly changing with temperature [70, 71, 72, 73, 74]. Then, it will be shown that particular ratios of the Polyakov loop susceptibilities reflect the underlying Z_3 center symmetry and can serve as observables to identify the onset of deconfinement in QCD

In the lattice QCD, the ultraviolet (UV) divergence of the free energy of bare quark in the continuum limit, and then the bare Polyakov loop vanishes at any temperature. Thus, the Polyakov loop must be renormalized so that it has a physically meaningful continuum limit. However, the renormalization of gluon correlation functions in general, and the Polyakov loop susceptibility in particular, still has uncertainties. Then, it will be that the ambiguities of the renormalization of the Polyakov loop are partially canceled in particular ratios of the Polyakov loop susceptibilities.

After we review the properties of the Polyakov loop fluctuations, and investigate the relation between confinement and chiral symmetry breaking in terms of the Polyakov loop fluctuations and their ratios. We derive the analytic relations between the real, imaginary and modulus of the Polyakov loop and their fluctuations and the Dirac modes on the temporally odd-number lattice with the periodic boundary condition. Then, we particularly consider the contribution of the low-lying Dirac modes to the Polyakov loop fluctuations.

Polyakov loop fluctuations

For each gauge configuration, by operating the Z_3 rotation the Polyakov loop (2.10), the Z_3 rotated Polyakov loop L is defined as

$$\tilde{L} = L\mathrm{e}^{2\pi ki/3} \tag{2.54}$$

with $k = 0, \pm 1$ [75, 76]. The variable k is determined so that $k = 0$ in the confined phase is taken, and k in the deconfined phase is taken such that the transformed Polyakov loop $\tilde{L}$ lies in its real sector. Using the Z_3 rotated Polyakov loop and its absolute value, the Polyakov loop susceptibilities are

defined as

$$T^3\chi_A = \frac{N_\sigma^3}{N_\tau^3}[\langle|L|^2\rangle - \langle|L|\rangle^2], \tag{2.55}$$

$$T^3\chi_L = \frac{N_\sigma^3}{N_\tau^3}[\langle(L_L)^2\rangle - \langle L_L\rangle^2], \tag{2.56}$$

$$T^3\chi_T = \frac{N_\sigma^3}{N_\tau^3}[\langle(L_T)^2\rangle - \langle L_T\rangle^2], \tag{2.57}$$

where $L_L \equiv \mathrm{Re}(\tilde{L})$ and $L_T \equiv \mathrm{Im}(\tilde{L})$, and consider their ratios,

$$R_A \equiv \frac{\chi_A}{\chi_L}, \tag{2.58}$$

$$R_T \equiv \frac{\chi_T}{\chi_L}. \tag{2.59}$$

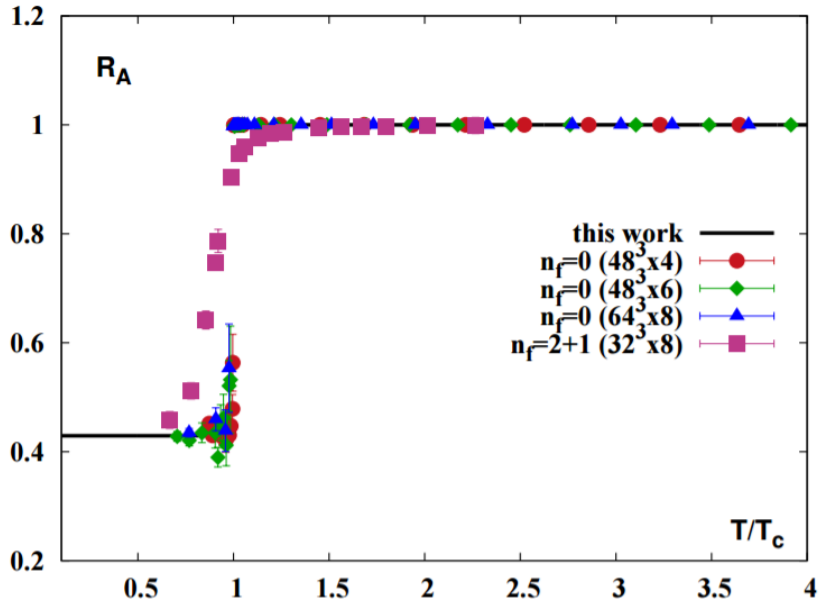

Figure 2.8: The temperature dependence of the ratio R_A. The lattice QCD simulations are performed at the quenched level and with the physical dynamical quarks. The temperature T is normalized by the deconfinement temperature T_c. The figure is taken from Ref. [76]

In particular, the ratio (2.58) of the Polyakov loop susceptibilities is important quantity. It is numerically shown to be robust probes of the deconfinement transition, shown in Fig. 2.8. It is almost temperature independent above and below the transition and there is a rapid change near the chiral crossover $T \simeq 150$. This characteristic behavior is understood in terms of the global Z_3 symmetry of the Yang-Mills Lagrangian and the general properties of the Polyakov loop probability distribution [75]. Moreover, the ambiguities of the renormalization of the Polyakov loop are partially canceled in the ratios. In fact, when renormalization of the Polyakov loop is multiplicative renormalization

$$L^{\rm ren} = Z(g^2)L, \tag{2.60}$$

the renormalization function $Z(g^2)$ is canceled in the ratios. Therefore, the ratios of the Polyakov loop susceptibilities are superior to the Polyakov loop itself.

In the following, we derive the analytical relations between the Polyakov loop fluctuations and the Dirac eigenmodes on the temporally odd-number lattice. And then, we both analytically and numerically investigate the contributions of the low-lying Dirac modes to the Polyakov loop fluctuation ratios.

The Polyakov loop fluctuations and Dirac modes

Next, we derive the relations between the Polyakov loop fluctuations and the Dirac modes. For simplicity, we consider the temporally odd-number lattice. We start the relation between the Polyakov loop and the Dirac modes (2.17). Since Eq. (2.17) is satisfied for each gauge-configuration, one can find the relation between the Z_3 transformed Polyakov loop $\tilde{L}$ and the Dirac modes,

$$\tilde{L} = \frac{(2ai)^{N_\tau-1}}{12V}\sum_n \lambda_n^{N_\tau-1} {\rm e}^{2\pi ki/3}\langle n|\hat{U}_4|n\rangle, \tag{2.61}$$

by multiplying Eq. (2.17) by the Z_3 factor ${\rm e}^{2\pi ki/3}$. Then, taking the real and the imaginary parts of Eq. (2.61), the longitudinal and transverse Polyakov loops can be expressed as

$$L_L = \frac{(2ai)^{N_\tau-1}}{12V}\sum_n \lambda_n^{N_\tau-1} {\rm Re}\left({\rm e}^{2\pi ki/3}\langle n|\hat{U}_4|n\rangle\right), \tag{2.62}$$

$$L_T = \frac{(2ai)^{N_\tau-1}}{12V}\sum_n \lambda_n^{N_\tau-1} {\rm Im}\left({\rm e}^{2\pi ki/3}\langle n|\hat{U}_4|n\rangle\right), \tag{2.63}$$

respectively. Also, by taking the absolute value of Eq. (2.17), the absolute value of the Polyakov loop can be written as

$$|L| = \frac{(2a)^{N_\tau-1}}{12V}\left|\sum_n \lambda_n^{N_\tau-1}\langle n|\hat{U}_4|n\rangle\right|. \tag{2.64}$$

Since Eqs. (2.61), (2.62), (2.63) and (2.64) are satisfied for each gauge configuration, the relations between them and the Dirac eigenmodes by substituting Eqs. (2.62)-(2.64) to Eqs. (2.55)-(2.57). In particular, the Dirac spectral representation of the $R_A = \chi_A/\chi_L$ ratio is expressed as

$$R_A = \frac{\left\langle\left|\sum_n \lambda_n^{N_\tau-1}\langle n|\hat{U}_4|n\rangle\right|^2\right\rangle - \left\langle\left|\sum_n \lambda_n^{N_\tau-1}\langle n|\hat{U}_4|n\rangle\right|\right\rangle^2}{\left\langle\left(\sum_n \lambda_n^{N_\tau-1}\mathrm{Re}\left(\mathrm{e}^{2\pi ki/3}\langle n|\hat{U}_4|n\rangle\right)\right)^2\right\rangle - \left\langle\sum_n \lambda_n^{N_\tau-1}\mathrm{Re}\left(\mathrm{e}^{2\pi ki/3}\langle n|\hat{U}_4|n\rangle\right)\right\rangle^2}. \tag{2.65}$$

Here, $\langle x\rangle$ denotes an average over all gauge configurations.

These relations (2.61)-(2.64) are satisfied both in full QCD and at the quenched level like the case of the Polyakov loop, namely Eq.(2.17). All these relations are derived on the temporally odd-number lattice for practical reasons. Of course, the relations on the even lattice can be derived by Eq. (2.23), and both choices of the parity for the lattice size in time direction give the same content of physics. However, the continuum limit is hard to practically perform. For example, the renormalization of the Polyakov loop has not been determined. Nevertheless, at least the ambiguity of the multiplicative renormalization of the Polyakov loop can be avoided by the cancellation of the renormalization function in the ratio of the Polyakov-loop susceptibilities [75, 76].

Numerical results

In order to numerically investigate the contribution of different Dirac modes to the Polyakov loop susceptibilities and their ratios, we use the above relations. Since the KS formalism can be applicable to the relations, we rewrite the relations using the formula $\langle n|\hat{U}_4|n\rangle = 4(n|\hat{U}_4|n)$.

We calculate the contributions from the low-lying Dirac modes to the Polyakov loop fluctuations using the SU(3) lattice QCD Monte Carlo simulations. The numerical setup is the same as the previous section. The Linear Algebra PACKage (LAPACK) [65] is used for diagonalization of the KS Dirac operator to obtain the eigenvalues λ_n and the eigenfunctions $\chi_n(s)$.

The lattice spacing a is determined by the string tension $\sigma = 0.89$ GeV/fm on a large lattice at each β at zero temperature. In this setup, in the confinement phase, the average of the plaquette is calculated as $\langle U_{\mu\nu}\rangle$=0.53(2). This is consistent with the previous SU(3) lattice studies [77]. In deconfined phase, the average value of plaquette is $\langle U_{\mu\nu}\rangle$=0.60(2), which is also consistent with the previous works [77]. For each value of $\beta = 5.6$ and $\beta = 6.0$, we use 20 gauge configurations, which are taken every 500 sweeps after the thermalization of 5000 sweeps.

Like the case of the Polyakov loop itself, the infrared cutoff Λ is introduced and we investigate the influence of the low-lying Dirac modes below Λ. Then, we introduce the Λ-dependent Polyakov loops,

$$|L|_\Lambda = \frac{(2a)^{N_\tau-1}}{3V}\left|\sum_{|\lambda_n|>\Lambda}\lambda_n^{N_\tau-1}(n|\hat{U}_4|n)\right|, \tag{2.66}$$

for the modulus, and

$$(L_L)_\Lambda = C_\tau \sum_{|\lambda_n|>\Lambda}\lambda_n^{N_\tau-1}\mathrm{Re}\left(\mathrm{e}^{2\pi ki/3}(n|\hat{U}_4|n)\right), \tag{2.67}$$

$$(L_T)_\Lambda = C_\tau \sum_{|\lambda_n|>\Lambda}\lambda_n^{N_\tau-1}\mathrm{Im}\left(\mathrm{e}^{2\pi ki/3}(n|\hat{U}_4|n)\right). \tag{2.68}$$

for the real and the imaginary part, respectively, with $C_\tau = (2ai)^{N_\tau-1}/3V$. Applying the cutoff dependent Polyakov loops from Eqs. (2.66), (2.67) and (2.68) to Eqs. (2.55)-(2.57), we also introduce the Λ-dependent susceptibilities

$$T^3(\chi_A)_\Lambda = \frac{N_\sigma^3}{N_\tau^3}[\langle|L|_\Lambda^2\rangle - \langle|L|_\Lambda\rangle^2] \tag{2.69}$$

$$T^3(\chi_L)_\Lambda = \frac{N_\sigma^3}{N_\tau^3}[\langle(L_L)_\Lambda^2\rangle - \langle(L_L)_\Lambda\rangle^2] \tag{2.70}$$

$$T^3(\chi_L)_\Lambda = \frac{N_\sigma^3}{N_\tau^3}[\langle(L_T)_\Lambda^2\rangle - \langle(L_T)_\Lambda\rangle^2], \tag{2.71}$$

where, and their ratios

$$(R_A)_\Lambda = \frac{(\chi_A)_\Lambda}{(\chi_L)_\Lambda}, \tag{2.72}$$

$$(R_T)_\Lambda = \frac{(\chi_T)_\Lambda}{(\chi_L)_\Lambda}. \tag{2.73}$$

In order to investigate the influence of the low-lying Dirac modes to the properties of the Polyakov loop fluctuations and the chiral condensate, we introduce two ratios. The cutoff-dependent chiral condensate $\langle\bar{q}q\rangle_\Lambda$ in Eq. (2.50) and the ratio

$$R_{\rm chiral} = \frac{\langle\bar{q}q\rangle_\Lambda}{\langle\bar{q}q\rangle} \tag{2.74}$$

for chiral symmetry breaking. In the same spirit, we introduce the ratio,

$$R_{\rm conf} = \frac{(R_A)_\Lambda}{R_A}\,, \tag{2.75}$$

in order to quantify the sensitivity of the Polyakov loop fluctuations to the particular Dirac modes. When, the ratio satisfies $R_{\rm conf} \simeq 1$, then the low-lying Dirac modes below the IR cutoff Λ are not essential to the Polyakov loop fluctuations.

The numerical results for the ratios $R_{\rm conf}$ and $R_{\rm chiral}$ in a confined phase at $\beta = 5.6$, for various values of the infrared cutoff Λ in Fig. 2.9. The ratio $R_{\rm chiral}$ is calculated with the quark mass $m = 5$ MeV. From the Fig. 2.9, it is found that the low-lying Dirac modes below Λ have the dominant contribution to the chiral condensate. Thus, the low-lying Dirac modes, which are important modes for chiral symmetry breaking. In contrast to $R_{\rm chiral}$, the $R_{\rm conf}$ ratio is almost unchanged by the removal of the low-lying Dirac modes even with relatively large cutoff $\Lambda \simeq 0.5$ GeV.

Thus, the important modes for chiral symmetry breaking are not important for confinement properties in QCD. In Table 2.5, the numerical results for the Polyakov loop fluctuations and IR cut fluctuations with the IR-cutoff $\Lambda \simeq 0.4$ GeV. In the deconfinement phase, the same behavior is observed as seen in Table 2.5.

Like the case of the Polyakov loop, we can analytically understand the differences in the influence of the low-lying Dirac modes on the chiral condensate and the Polyakov loop fluctuations. Due to the damping factor $\lambda_n^{N_\tau-1}$, the contributions from the low-lying Dirac modes are strongly suppressed for the Polyakov loops, $|L|$, L_L, L_T from Eqs. (2.62)-(2.64) because the Dirac matrix element $\langle n|\hat{U}_4|n\rangle$ is finite. Then, since the susceptibilities and their ratios are defined from the Polyakov loops, the low-lying Dirac modes have the negligible contributions to them, too. Thus, the essential modes for chiral symmetry breaking are not essential for a sensitive probe R_A for deconfinement in QCD. This result suggests no direct one-to-one correspondence between confinement and chiral symmetry breaking in QCD. In this way, we have improved the discussion in the previous section by considering the Polyakov loop fluctuations.

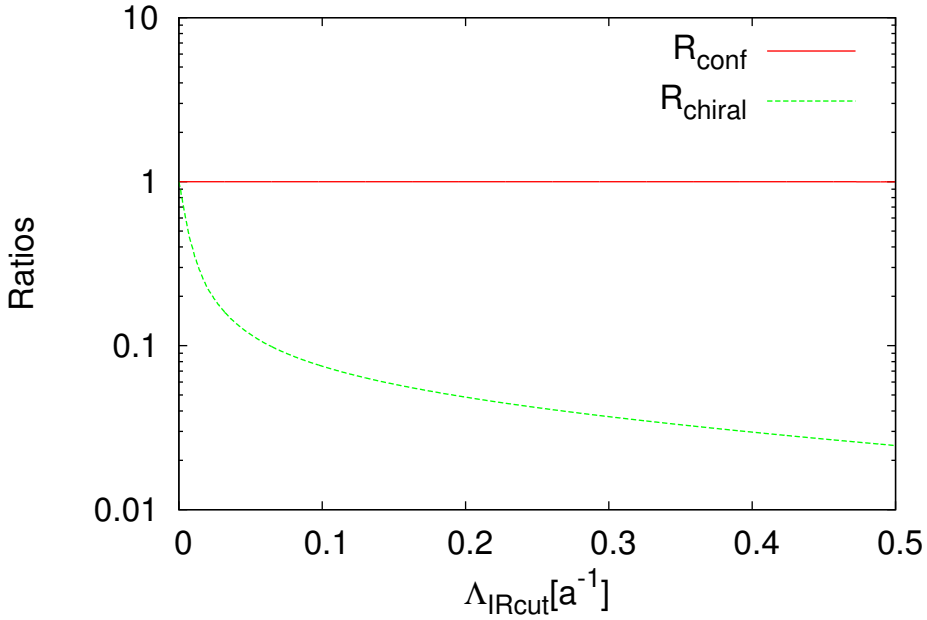

Figure 2.9: The numerical results for the ratios R_{chiral} and R_{conf} from Eqs. (2.74) and (2.75), respectively, as a function of an infrared cutoff Λ introduced on Dirac eigenvalues, expressed in the lattice unit. The Monte Carlo calculations have been performed on the $10^3 \times 5$ lattice with $\beta = 5.6$, and for the quark mass of $m = 5$ MeV. This figure is taken from Ref. [66].

Table 2.5: Numerical results for the original values of the Polyakov-loop fluctuations, and IR cut fluctuations with the IR-cutoff $\Lambda \simeq 0.4$ GeV. The results are obtained in quenched QCD on $10^3 \times 5$ lattice with $\beta = 5.6$ (confined phase) and $\beta = 6.0$ (deconfined phase) with 20 gauge configurations. This table is essentially same as that in Ref. [66].

β		original	IR-cut
β=5.6	$T^3\chi_A$	3.475×10^{-4}	3.470×10^{-4}
	$T^3\chi_L$	5.307×10^{-4}	5.298×10^{-4}
	$T^3\chi_T$	6.005×10^{-4}	5.994×10^{-4}
	R_A	0.6548	0.6549
	R_T	1.131	1.131
β=6.0	$T^3\chi_A$	2.965×10^{-3}	2.965×10^{-3}
	$T^3\chi_L$	3.015×10^{-3}	3.015×10^{-3}
	$T^3\chi_T$	7.848×10^{-4}	7.848×10^{-4}
	R_A	0.9834	0.9834
	R_T	0.2603	0.2603

2.3 Wilson loop

In this section, we derive a formula to express the Wilson loop in terms of the Dirac eigenmodes [62]. In addition to the Polyakov loop and its fluctuations, the Wilson loop is also important quantity for quark-confinement because interquark potential can be defined from the Wilson loop. The formula is valid on an arbitrary square lattice, unlike the formulae for the Polyakov loops. In the following, we show the detailed derivation.

We consider the Wilson loop $W(R,T)$ corresponding to a rectangular loop with $R \times T$, shown in Fig. 2.10. It can be expressed as the functional trace

$$W(R,T) \equiv \mathrm{Tr}_c \left[\hat{U}_1^R \hat{U}_{-4}^T \hat{U}_{-1}^R \hat{U}_4^T \right] = \mathrm{Tr}_c \left[\hat{S} \hat{U}_4^T \right], \tag{2.76}$$

where $\hat{S}$ is the "staple operator" defined as

$$\hat{S} \equiv \hat{U}_1^R \hat{U}_{-4}^T \hat{U}_{-1}^R. \tag{2.77}$$

Like the formula (2.17) for the Polyakov loop, that for the Wilson loop can be derived by introducing a particular functional trace, showing that it is proportional to the Wilson loop, and expanding it with the Dirac eigenmodes.

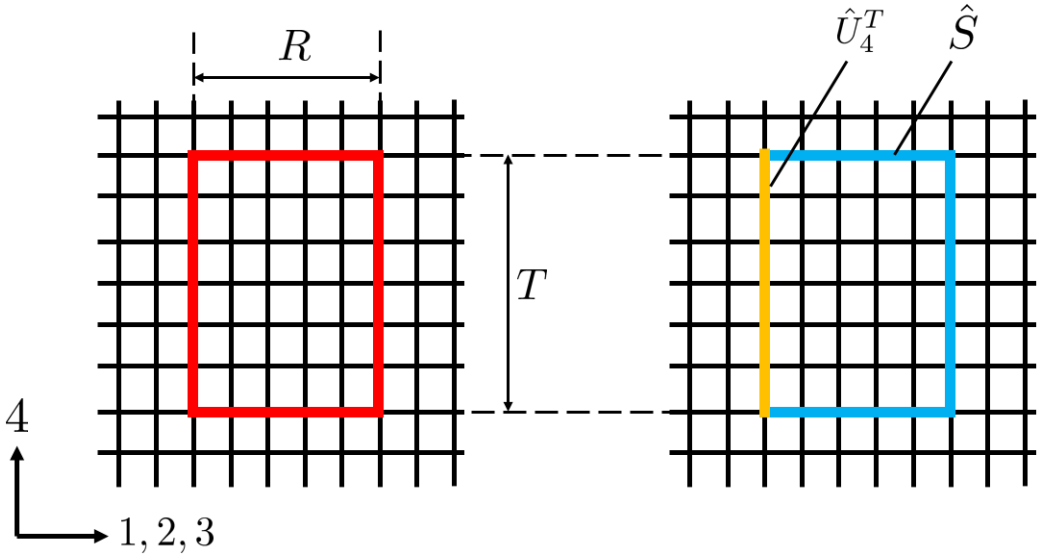

Figure 2.10: (Left) A rectangular loop with $R \times T$ on the square lattice corresponding to the Wilson loop $W(R,T)$. (Right) The loop is decomposed to the two parts, the staple $\hat{S}$ and the temporal line $\hat{U}_{-4}^T$.

For simplicity, we consider even number T. The functional trace is introduced as

$$J \equiv \mathrm{Tr}_{c,\gamma} \hat{S} \hat{\not{D}}^T, \tag{2.78}$$

where $\hat{\not{D}}$ is given in Eq. (2.3). It corresponds to Eq. (2.14) in section 2.1. We can show that the quantity includes only the Wilson loop. Here, we note that the distance between the end points of the staple operator is T, and the Dirac operator $\hat{\not{D}}$ is expressed as the linear combination of the link-variable operators. Thus, only the $\hat{U}_4^T$ term in the expansion of $\hat{\not{D}}^T$ is only the gauge-invariant term corresponding to the closed loop, namely the Wilson loop.

Therefore, we can obtain

$$\begin{aligned} J &= \mathrm{Tr}_{c,\gamma}\hat{S}\hat{\not{D}}^T \\ &= \mathrm{Tr}_{c,\gamma}\hat{S}(\gamma_4\hat{D}_4)^T \\ &= 4\mathrm{Tr}_c\hat{S}\hat{D}_4^T \\ &= \frac{4}{(2a)^T}\mathrm{Tr}_c\hat{S}(\hat{U}_4 - \hat{U}_{-4})^T \\ &= \frac{4}{(2a)^T}\mathrm{Tr}_c\hat{S}\hat{U}_4^T \\ &= \frac{4}{(2a)^T}W. \end{aligned} \tag{2.79}$$

On the other hand, when the Dirac mode is taken as the basis for the functional trace, J is expressed as

$$J = \sum_n \langle n|\hat{S}\hat{\not{D}}^T|n\rangle = (-)^{\frac{T}{2}}\sum_n \lambda_n^T\langle n|\hat{S}|n\rangle, \tag{2.80}$$

where we use the eigenvalue equation (2.4). In this way, we obtain the relation

$$W(R,T) = \frac{(-)^{\frac{T}{2}}(2a)^T}{4}\sum_n \lambda_n^T\langle n|\hat{S}|n\rangle \tag{2.81}$$

for even T. We again note that the low-lying Dirac mode contributions to the Wilson loop is expected to be negligible compared to the other higher modes due to the damping factor λ_n^T. Although the matrix element $\langle n|\hat{S}|n\rangle$ has the explicit T-dependence, the absolute value is finite, and then it does not disturb the argument.

Of course, the similar analysis can be performed in the case of odd number T. In fact, instead of J, when we consider the functional trace for odd T

$$K \equiv \mathrm{Tr}_{c,\gamma}\hat{S}\hat{U}_4\hat{\not{D}}^{T-1}, \tag{2.82}$$

we can calculate

$$\begin{aligned} K &= \mathrm{Tr}_{c,\gamma}\hat{S}\hat{U}_4\hat{\not{D}}^{T-1} \\ &= \mathrm{Tr}_{c,\gamma}\hat{S}\hat{U}_4(\gamma_4\hat{D}_4)^{T-1} \\ &= \frac{4}{(2a)^{T-1}}\mathrm{Tr}_c\hat{S}\hat{U}_4(\hat{U}_4 - \hat{U}_{-4})^{T-1} \\ &= \frac{4}{(2a)^{T-1}}\mathrm{Tr}_c\hat{S}\hat{U}_4^T \\ &= \frac{4}{(2a)^{T-1}}W, \end{aligned} \tag{2.83}$$

and

$$\begin{aligned} K &= \sum_n \langle n|\hat{S}\hat{U}_4 \not{D}^{T-1}|n\rangle \\ &= (-)^{\frac{T-1}{2}} \sum_n \lambda_n^{T-1} \langle n|\hat{S}\hat{U}_4|n\rangle. \end{aligned} \tag{2.84}$$

Therefore, the similar formula holds for the odd T as

$$W = \frac{(-)^{\frac{T-1}{2}}(2a)^{T-1}}{4} \sum_n \lambda_n^{T-1} \langle n|\hat{S}\hat{U}_4|n\rangle. \tag{2.85}$$

The indication from Eq. (2.85) is the same as that from Eq. (2.81). That is, the low-lying Dirac modes have little contribution to the Wilson loop.

The $\bar{q}q$ potential $V(R)$ is considered in terms of the Dirac modes using the relation connecting the Wilson loop and the Dirac modes. We consider even T case. In the large T limit, the interquark potential $V(R)$ is extracted as

$$V(R) = -\lim_{T\to\infty} \frac{1}{T} \ln\langle W(R,T)\rangle. \tag{2.86}$$

Since now the Wilson loop is expressed by the Dirac modes and the relation is valid for arbitrary gauge configuration, the potential $V(R)$ can be expressed as

$$V(R) = -\lim_{T\to\infty} \frac{1}{T} \ln \left| \left\langle \sum_n (2a\lambda_n)^T \langle n|\hat{S}|n\rangle \right\rangle \right|. \tag{2.87}$$

Similarly, the string tension σ can be expressed as

$$\begin{aligned} \sigma &= -\lim_{R,T\to\infty} \frac{1}{RT} \ln\langle W\rangle \\ &= -\lim_{R,T\to\infty} \frac{1}{RT} \ln \left| \left\langle \sum_n (2a\lambda_n)^T \langle n|\hat{S}|n\rangle \right\rangle \right|. \end{aligned} \tag{2.88}$$

Again because of the damping factor λ_n^T in the sum, we can find that both the $\bar{q}q$ potential $V(R)$ and the string tension σ are not almost affected by the low-lying Dirac modes unless $\langle n|\hat{S}|n\rangle$ has a counter factor such as λ_n^{-T}. Also for odd T case, similar arguments can be done with Eq.(2.85). Therefore, we directly confirm that the string tension σ, or the confining force, is almost unchanged even if the low-lying Dirac modes disappear, which means chiral symmetry restoration.

Chapter 3

Generalization to chiral fermion on the lattice

In this chapter, we generalize the previous discussion for the relation between the Polyakov loop and the Dirac eigenmodes. As mentioned in section 1.4, the fermionic action $a^4 \sum_s \bar{q}(s) \left(D_{\rm Lat} + m\right) q(s)$, equivalently the Dirac operator $D_{\rm Lat}$ on the lattice, is complicated due to the fermion doubling problem. This problem is usually avoided by explicitly breaking the chiral symmetry, which is one of the conditions for the Nielsen-Ninomiya theorem [12, 35, 36]. In fact, the naive Dirac operator $\hat{\not{D}}$, which is used in the above chapter, includes the fermion doubler modes, and their contributions must be removed. Since the analytical relations are nontrivial between the Polyakov loop and the eigenmodes of the Dirac operators which explicitly break the chiral symmetry on the lattice, we discuss the relations in this chapter.

First of all, we review the Wilson, Wilson-clover, and overlap fermion formalism as the lattice Dirac operators. Second, the relation between the Polyakov loop and the Wilson(-clover)-Dirac modes is analytically derived. Finally, we discuss the relation between quark-confinement and chiral symmetry breaking in QCD using the overlap-Dirac operator, which is referred to as chiral fermion.

3.1 Lattice fermion and fermionic doubler modes

The Wilson fermion is the simplest lattice fermion which can avoid the doubling problem [12, 33]. The fundamental idea of the Wilson fermion is to give the heavy masses to the doublers modes. The Wilson-Dirac operator is

given by

$$\hat{D}_{\mathrm{W}} = \hat{\not{D}} - \frac{ar}{2}\hat{D}^2, \tag{3.1}$$

The first term $\not{D} \equiv D_\mu \gamma_\mu$ is the naive discretization of the Dirac operator, and the second term is the Wilson term. The real parameter r is referred to as the Wilson parameter, and it is usually set $r = 1$. Using the covariant derivative on the lattice

$$\langle s|\hat{D}_\mu|s'\rangle = \frac{1}{2a}\left(U_\mu(s)\delta_{s+\hat{\mu},s'} - U_{-\mu}(s)\delta_{s-\hat{\mu},s'}\right), \tag{3.2}$$

and the center discretization for D^2, the Wilson-Dirac operator is

$$\begin{aligned}&\langle s|\hat{D}_{\mathrm{W}}|s'\rangle \\ &\quad = 4ar - \frac{1}{2a}\sum_\mu \left[(1-\gamma_\mu)U_\mu(s)\delta_{s+\hat{\mu},s'} - (1+\gamma_\mu)U_{-\mu}(s)\delta_{s-\hat{\mu},s'}\right].\end{aligned} \tag{3.3}$$

The Wilson-Dirac operator approaches the continuum Dirac operator with $\mathcal{O}(a)$. In the case of the free fermion, the quark propagator in the momentum space is

$$\langle \bar{q}_\alpha(s_1) q_\beta(s_2)\rangle = \int_{-\frac{\pi}{a}}^{\frac{\pi}{a}} \frac{d^4p}{(2\pi)^4} \frac{(-i\gamma_\mu \tilde{\tilde{p}}_\mu + M(p))_{\alpha\beta}}{\sum_\mu (\tilde{\tilde{p}}_\mu)^2 + M(p)^2} \mathrm{e}^{ip(s_1-s_2)a}, \tag{3.4}$$

where $\tilde{\tilde{p}}_\mu = \frac{1}{a}\sin(p_\mu a)$ and

$$M(p) \equiv M + \frac{2r}{a}\sum_\mu \sin^2(p_\mu a/2). \tag{3.5}$$

The second term is contribution from the Wilson term and increases as $1/a$ with the continuum limit $a \to 0$ when $p_\mu a \neq$ poles, corresponding to the doubler modes. Then, the doubler modes obtain large masses at the continuum limit and do not contribute to the low-energy physics. In this way, the Wilson fermion formalism solves the doubling problem.

The Wilson-Dirac operator can be improved by the adding the space-diagonal term referred to as the clover term

$$A(s) = -\frac{1}{2}c_{\mathrm{SW}}\sum_{\mu<\nu}\left[\gamma_\mu, \gamma_\nu\right] F_{\mu\nu}(s), \tag{3.6}$$

where the parameter c_{SW} is set as $c_{\mathrm{SW}} = 1$ at the tree level, and the field strength tensor $F_{\mu\nu}(s)$ on the lattice is defined as

$$F_{\mu\nu}(s) = \frac{1}{8}\left(P_{\mu\nu}(s) - P_{\mu\nu}^\dagger(s)\right) \tag{3.7}$$

with

$$
\begin{aligned}
P_{\mu\nu}(s) = & U_\mu(s)U_\nu(s+\hat{\mu})U_\mu^\dagger(s+\hat{\nu})U_\nu^\dagger(s) \\
& + U_\nu(s)U_\mu^\dagger(s-\hat{\mu}+\hat{\nu})U_\nu^\dagger(s-\hat{\nu})U_\mu(s-\hat{\nu}) \\
& + U_\mu^\dagger(s-\hat{\mu})U_\nu^\dagger(s-\hat{\mu}-\hat{\nu})U_\mu(s-\hat{\mu}-\hat{\nu})U_\nu(s-\hat{\nu}) \\
& + U_\nu^\dagger(s-\hat{\nu})U_\mu(s-\hat{\nu})U_\nu(s+\hat{\mu}-\hat{\nu})U_\mu^\dagger(s).
\end{aligned} \tag{3.8}
$$

The improved Dirac operator is referred to as the clover-Wilson-Dirac operator. The origin of the name of the clover-term comes from the form of Eq. (3.8), shown in Fig. 3.1.

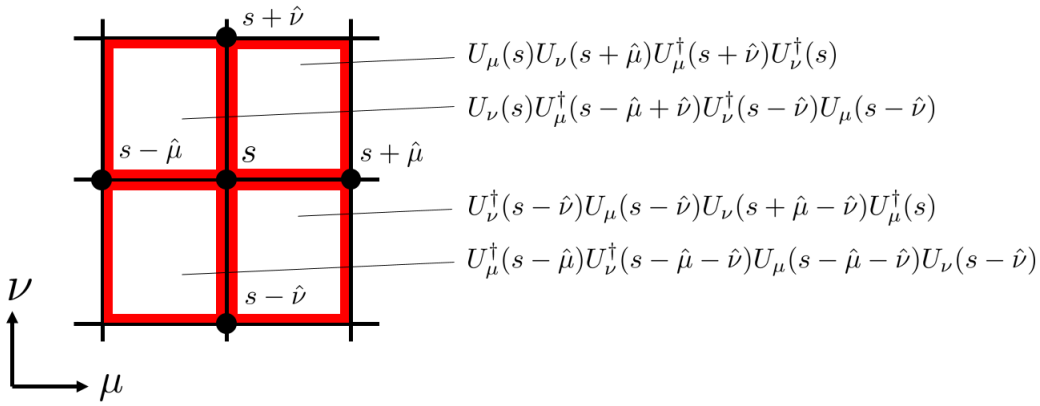

Figure 3.1: Clover-like structure of the quantity $P_{\mu\nu}(s)$ of Eq. (3.8) on a square lattice. The red squares express the corresponding terms in Eq. (3.8).

The Wilson type of the Dirac operator on the lattice explicitly breaks the chiral symmetry in order to avoid the doubling problem. However, the chiral symmetry and its spontaneous breaking are important for the low-energy dynamics on QCD, and thus the chiral symmetry is expected to be maximally respected. Based on this concept, the Ginsparg-Wilson (GW) relation is derived [78]. If the lattice Dirac operator D on a lattice satisfies the GW relation

$$
\gamma_5\hat{D} + \hat{D}\gamma_5 = a\hat{D}\gamma_5\hat{D}, \tag{3.9}
$$

the lattice action $S_{\rm F} = \bar{q}Dq$ has the exact symmetry on the lattice. The infinitesimal transformation operating the fermionic fields associated with the exact symmetry is

$$
\delta q = \gamma_5(1 - \frac{1}{2}a\hat{D})q, \qquad \delta q = \bar{q}(1 + \frac{1}{2}a\hat{D})\gamma_5. \tag{3.10}
$$

The transformation (3.10) approaches the axial transformation with the continuum limit $a \to 0$. In this sense, the lattice-Dirac operator satisfying the GW relation is the best Dirac operator on the lattice because it solves the fermion doubling problem with approximate chiral symmetry, which is maximally realized on the lattice.

One of the Dirac operator satisfying the GW relation is the overlap-Dirac operator $D_{\rm ov}$ [79] defined as

$$\hat{D}_{\rm ov} = \frac{1}{a}\left[1 + \frac{\hat{D}_{\rm W}(-M_0)}{\sqrt{\hat{D}^{\dagger}_{\rm W}(-M_0)\hat{D}_{\rm W}(-M_0)}}\right], \tag{3.11}$$

where $D_{\rm W}(-M_0)$ is the Wilson-Dirac operator with the negative mass term $(-M_0)$. If one adjusts the negative mass, the contribution from doubler modes are decoupled from the low-energy dynamics in the continuum limit. In the case of the free fermion, the condition is M_0 as $0 < M_0 < 2$ [79]. The overlap-Dirac operator satisfies the GW relation (3.9) [80]:

$$\gamma_5 \hat{D}_{\rm ov} + \hat{D}_{\rm ov}\gamma_5 = a\hat{D}_{\rm ov}\gamma_5\hat{D}_{\rm ov}. \tag{3.12}$$

3.2 The relation between Polyakov loop and low-lying modes of overlap-Dirac operator

Fist of all, we derive the analytical relation connecting the Polyakov loop and the Wilson-Dirac modes. The main motivation is eliminating the fermion doubling problem and ensuring the correct continuum limit. The relation will be used for the discussion for the overlap-Dirac modes.

The relation between Polyakov loop and Wilson-Dirac modes

Using the link-variable operators, the Wilson-Dirac operator is given as

$$\hat{D}_{\rm W} = 4r/a - \frac{1}{2a}\sum_{\mu=1}^{4}\left[(r-\gamma_\mu)\hat{U}_\mu + (r+\gamma_\mu)\hat{U}_{-\mu}\right]. \tag{3.13}$$

While the Dirac operator (2.3) is anti-hermitian, the Wilson-Dirac operator (3.13) is neither hermitian nor anti-hermitian. Thus, the eigenvalue equation of the Wilson-Dirac operator is written as

$$\hat{D}_{\rm W}|n\rangle_{\rm W} = \Lambda^{\rm W}_n|n\rangle_{\rm W}, \tag{3.14}$$

where $\Lambda_n \in \mathbf{C}$. Note that these Wilson-Dirac mode is not complete system. However, the explicit breaking of the anti-hermiticity is $\mathcal{O}(a)$, it is almost complete set with sufficient small lattice spacing.

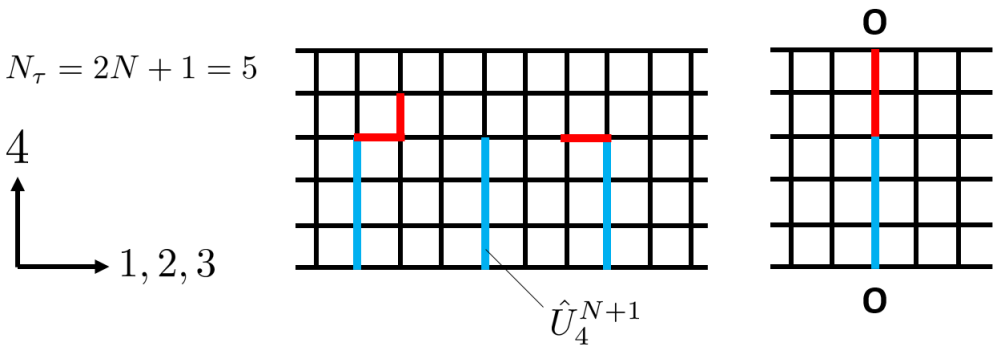

Figure 3.2: An example of odd lattice. This is $N_\tau = 2N + 1 = 5$ case. The blue line corresponds to the operator $\hat{U}_4^{N+1}$ in Eq. (3.20), and the red line corresponds to the link-variable operator $\hat{U}_\mu$. Due to the diagonal term in the (clover-)Wilson-Dirac operator, the length l of each line is in the range $N + 1 \leq l \leq N_\tau$. The The Polyakov loop is the unique closed loop using the temporal periodicity. All the lines in the left figure correspond to the gauge-variant terms while the line in the right figure is the unique closed loop using the temporal periodicity, namely the Polyakov loop.

We again consider the temporally odd-number lattice and we set the temporal size as $N_\tau = 2N + 1$. The derivation of the relation between the Polyakov loop and the Wilson-Dirac modes is the essentially same as the derivation of Eq. (2.23). The single difference is the degree of the link-variable operator. We introduce the functional trace I_{W}

$$I_{\mathrm{W}} \equiv \mathrm{Tr}_{c,\gamma}(\hat{U}_4^{N+1}\hat{D}_{\mathrm{W}}^N) \tag{3.15}$$

with the functional trace $\mathrm{Tr}_{c,\gamma} \equiv \sum_s \mathrm{tr}_c$. From Eq.(3.13), each term in the expansion of $\hat{U}_4^{N+1}\hat{D}_{\mathrm{W}}^N$ has products of n link-variable operators, where $N+1 \leq n \leq 2N+1 (= N_\tau)$. Here, we note two points. The first point is that any closed loops cannot be made using odd-number link-variable operators on a square lattice. The second point is that the possible closed loop is the Polyakov loop using the temporal periodic boundary condition because the number of $\hat{U}_4$ is larger that of $\hat{U}_{-4}$. Therefore, we conclude that the quantity

$I_{\rm W}$ is proportional to the Polyakov loop. The total derivation is

$$\begin{aligned} I_{\rm W} &= {\rm Tr}_{c,\gamma}(\hat{U}_4^{N+1}\hat{D}_{\rm W}^N) \\ &= \frac{1}{(2a)^N}{\rm Tr}_{c,\gamma}(\hat{U}_4^{N+1}(r-\gamma_4)^N\hat{U}_4^N) \\ &= \frac{1}{(2a)^N}{\rm Tr}_c(\hat{U}_4^{N_\tau}){\rm tr}_\gamma[(r-\gamma_4)^N] \\ &= -\frac{3V}{(2a)^N}\left(\sum_{n=0}^{N} {}_NC_n r^n {\rm tr}_\gamma[(\gamma_4)^{N-n}]\right) L. \end{aligned} \tag{3.16}$$

If we set the ordinary value $r = 1$ of the Wilson parameter, the above relation becomes simpler as

$$I_{\rm W} = \frac{3V}{2a^N}L \tag{3.17}$$

because $(\gamma_4)^2 = 1$, ${\rm tr}_\gamma\gamma_4 = 0$ and $\sum_{n=0}^{N} {}_NC_n = 2^{N-1}$. In the following, we use $r = 1$.

On the other hand, taking the Wilson-Dirac modes as the basis for the functional trace in Eq.(3.20), we find

$$\begin{aligned} I_{\rm W} &= \sum_n \langle n|\hat{U}_4^{N+1}\hat{D}_{\rm W}^N|n\rangle_{\rm W} \\ &= \sum_n (\Lambda_n^{\rm W})^N \langle n|\hat{U}_4^{N+1}|n\rangle_{\rm W}, \end{aligned} \tag{3.18}$$

where we abbreviate the bra-vector ${}_{\rm W}\langle n|$ to $\langle n|$.

Combining Eqs.(3.17) and (3.18), we obtain

$$L = -\frac{2a^N}{3V}\sum_n (\Lambda_n^{\rm W})^N \langle n|\hat{U}_4^{N+1}|n\rangle_{\rm W}. \tag{3.19}$$

This analytical relation connects the Polyakov loop and the Wison-Dirac modes. Note that the clover term is diagonal in the space-time space, and then the relation (3.19) is satisfied with the clover-Wilson-Dirac operator.

The relation between Polyakov loop and low-lying modes of overlap-Dirac operator

The overlap-Dirac operator is expressed as the infinite series in terms of the link-variable operator while the naive-Dirac operator $\hat{\not{D}}$ and the Wilson-Dirac operator $\hat{D}_{\rm W}$ include only the linear terms. Thus, it is difficult to

directly show the analytical formula connecting the Polyakov loop and the eigenmodes of the overlap-Dirac operator by the similar method in the case of $\hat{\not{D}}$ and $\hat{D}_{\rm W}$. Nevertheless, their relation can be understood through the eigenmodes of the Wilson-Dirac operator, and it is explained in the following.

We explain why it is difficult to derive the direct relation connecting the Polyakov loop and the overlap-Dirac modes. Consider the expansion of the overlap-Dirac operator. If the overlap-Dirac operator has finite terms with finite degrees of the link-variable operators, we can derive the analytical formula by considering

$$I_{\rm ov} \equiv {\rm Tr}_{c,\gamma}(\hat{U}_4^{N+1}\hat{D}_{\rm ov}^N) \tag{3.20}$$

with sufficiently large N. However, it is found from the GW relation (3.12) that the overlap-Dirac operator is infinite series of the link-variable operators because the highest degree in RHS is larger than the highest degree in LHS. Then, the method in the case of the Polyakov loop and Wilson loop using the naive or Wilson-Dirac operator is not applicable to the case of the overlap-Dirac operator.

The eigenvalue equation of the overlap-Dirac operator is written as

$$\hat{D}_{\rm ov}|n\rangle_{\rm ov} = \Lambda_n^{\rm ov}|n\rangle_{\rm ov}, \tag{3.21}$$

where $\Lambda_n^{\rm ov} \in \mathbf{C}$ is the eigenvalue. Since the overlap-Dirac operator satisfies the GW relation and γ_5-hermiticity, The eigenvalues $\Lambda_n^{\rm ov}$ of the overlap-Dirac operator are distributed on a circle in the complex plane which has the center $(1/a, 0)$ and the radius $1/a$, shown in Fig. 3.3. In particular, the eigenmodes around the origin $(0, 0)$ correspond to physical modes while eigenmodes around the point $(2/a, 0)$ correspond to doubler's modes. In fact, in the continuum limit, the former approach the eigenmodes of the continuum Dirac operator while the latter is decoupled from the low-energy physics because of divergence of the radius of the circle. Moreover, the chiral condensate $\langle\bar{q}q\rangle$ is expressed by the overlap-Dirac modes as

$$\langle\bar{q}q\rangle = -\frac{1}{V}\sum_n \frac{1}{\Lambda_n^{\rm ov} + m}, \tag{3.22}$$

where m is the current quark mass. The low-lying modes ($|\Lambda_n^{\rm ov}| \ll 1$) of the overlap-Dirac modes have large contribution to the chiral condensate, which is the order parameter of chiral symmetry breaking. Thus, the low-lying overlap-Dirac modes are physical and essential for chiral symmetry breaking.

The eigenmodes of the Wilson-Dirac operator can be obtained, and the eigenvalues $\Lambda_n^{\rm W}$ of the Wilson-Dirac operator $D_{\rm W}(-M_0)$ are shown in Fig.

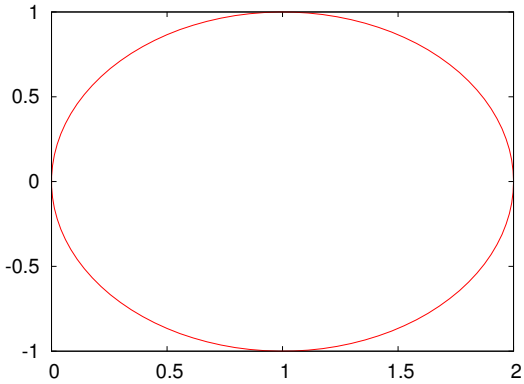

Figure 3.3: The distribution of the eigenvalues $\Lambda_n^{\rm ov}$ of the overlap-Dirac operator. The eigenvalues are distributed on the circle with the center $(1/a, 0)$ and the radius $1/a$. In this figure, we set a=1.

3.4, where we set $M_0 = 1.6$ [82] in the lattice unit. In the eigenvalue distribution, there are 5 types of the real modes whose eigenvalues are real. Among these modes, the modes which have the negative real eigenvalues correspond to the physical near-zero modes while other real modes correspond to the doubler modes. Moreover, one can adjust the location of the physical mode so that the eigenvalue $\tilde{\Lambda}_n^{\rm W} \in \mathbf{R}$ lie in the range $-1 \leq \tilde{\Lambda}_n^{\rm W} \leq 0$ by varying M_0. Thus, from the view point of the physical and doubler modes, the low-lying modes of the Wilson-Dirac and overlap-Dirac operators correspond each other.

The correspondence between the low-lying eigenmodes of the overlap-Dirac operator and the Wilson-Dirac operator can be understood by another way. If a general matrix M is normal, matrices $M' \equiv \frac{M}{\sqrt{M^\dagger M}}$ and M have the same eigenvectors and the relation of their eigenvalues can be expressed as

$$m' = \frac{m}{|m|}, \tag{3.23}$$

where m' and m are the eigenvalues of M' and M, respectively. However, since the Wilson-Dirac operator is not normal, the relation of the eigenvalues $\Lambda_n^{\rm ov}$ and $\Lambda_n^{\rm W}$ is nontrivial. Nevertheless, the their relation is expected to be expressed as

$$\Lambda_n^{\rm ov} = \frac{1}{Ra}\left(1 + \frac{\Lambda_n^{\rm W}}{|\Lambda_n^{\rm W}|}\right) + \mathcal{O}(a) \tag{3.24}$$

because the breaking of the normality of the Wilson-Dirac operator is caused by the so-called Wilson term and its amplitude is $\mathcal{O}(a)$. As long as the

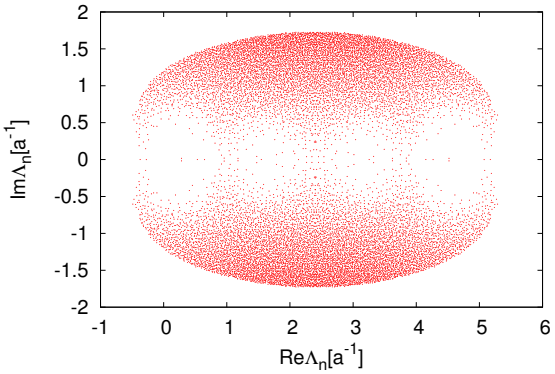

Figure 3.4: The distribution of the eigenvalues $\Lambda_n^{\rm W}$ of the Wilson-Dirac operator $\hat{D}_{\rm W}(-M_0)$, where we set $M_0 = 1.6$ in the lattice unit. The gauge-configuration is generated in the quenched simulation on 6^4 lattice with $\beta = 5.6$.

continuum limit is interested in, Eq. (3.24) can be regarded approximately satisfied. A notable point about Eq. (3.24) is that an eigenvalue $\Lambda_n^{\rm W}$ of the Wilson-Dirac operator corresponds to the unique eigenvalue $\Lambda_n^{\rm ov}$ of the overlap-Dirac operator while an eigenvalue $\Lambda_n^{\rm ov}$ determines the only phase θ_n of the eigenvalue $\Lambda_n^{\rm W}$, where the phase θ_n is defined by $\Lambda_n^{\rm W} = |\Lambda_n^{\rm W}|e^{i\theta_n}$ $(0 \leq \theta_n < 2\pi)$. In particular, the low-lying Dirac modes of the overlap-Dirac operator are correspond to the Wilson-Dirac modes whose phases are around π. By adjusting the negative mass M_0, these modes with $\theta_n \simeq \pi$ can have the small absolute values $(|\Lambda_n^{\rm W}| < 1)$. Thus, the low-lying overlap-Dirac modes correspond to the Wilson-Dirac modes whose eigenvalues of the absolute value are relatively small.

The above discussion is summarized as the three important points:

- the low-lying overlap-Dirac modes are essential for chiral symmetry breaking.
- the low-lying overlap-Dirac modes correspond to the low-lying Wilson-Dirac modes.
- the low-lying Wilson-Dirac modes have little contribution to the Polyakov loop.

The first point is confirmed by the Dirac representation of the chiral condensate, Eq (3.22). The second point is confirmed from the consideration

for the eigenvalue distributions of the Wilson-Dirac and overlap-Dirac operators in the view point of the correspondence of the fermionic doubler modes. The 3rd point was confirmed by the formula (3.19) connecting the Polyakov loop and the Wilson-Dirac modes. From these points, therefore, the presence or absence of the low-lying overlap-Dirac modes is not related to the value of the Polyakov loop while the chiral condensate is sensitive to that. This result indicates that there is no direct, one-to-one correspondence between confinement and chiral symmetry breaking in QCD.

Chapter 4

Summary and Outlook

In this thesis, we have discussed the relation between the non-perturbative phenomena, such as quark-confinement and chiral symmetry breaking using the relations connecting order parameters for quark confinement and the eigenmodes of the Dirac operators in the lattice QCD. In the following, we summarize our study and present an outlook in this context.

Using the naive Dirac operator on the temporally odd-number lattice, where the temporal lattice size is odd number with the proper periodic boundary condition, the analytical relation connecting the Polyakov loop and the Dirac eigenmodes is derived. This analytical relation can be generalized to the even lattice, where all the lattice sizes are even number. These analytical relations indicate that the low-lying Dirac eigenmodes have the negligible contributions to the Polyakov loop. Then, this observation means that the important modes for chiral symmetry breaking are not important for quark-confinement. This is also numerically confirmed by the lattice QCD calculations. After removal of the low-lying Dirac modes below the infrared scale $\Lambda_{\rm IR} \sim 400$ MeV, the Polyakov loop is almost unchanged. Moreover, from the analysis for the Dirac matrix element of the link-variable appearing in the analytical relation, there is a new symmetry, which we refer as to the "positive/negative" symmetry. This symmetry is realized in the confined phase, and then the contributions from arbitrary range of the Dirac eigenvalues are canceled due to this symmetry. Although the behavior of the new symmetry is similar to the center symmetry, the origin of the new symmetry has not been revealed yet. Thus, it is interesting to investigate the relation between the positive/negative symmetry and the center symmetry because both symmetries are very related to confinement property.

Next, we improve the above discussion by considering the Polyakov loop fluctuations. In particular, the specific ratio R_A is a very sensitive probe for the onset of the deconfinement transition of quarks. The Dirac spectrum

representations for the Polyakov loop fluctuations can be derived, and it is numerically confirmed that the low-lying Dirac modes have the negligible contributions to the Polyakov loop fluctuations. The Wilson loop is also expressed by the Dirac eigenmodes. Due to the damping factor, the contributions from the low-lying Dirac modes to the Wilson loop are strongly suppressed. Since the interquark potential is calculated from the Wilson loop, this observation indicates that the linear confining potential of the quark-antiquark system is not related with the density of the low-lying Dirac modes.

The various quantities, namely the Polyakov loop and its fluctuations, and the Wilson loop, which are relevant to quark-confinement, are not almost influenced by whether the Dirac operator has the low-lying modes, or not. Then, it is expected that the confinement property of the QCD vacuum is always not directly affected by the chiral symmetry breaking and its restoration. However, the quark-deconfinement and the chiral restoration almost simultaneously occur at finite temperature. Unfortunately, the reason of this coincidence of the critical temperatures has not been explained, and thus the problem still remains. Moreover, other quantities such as the quark scalar charge [27, 28] and the kurtosis of the net-quark number fluctuations [83, 84, 85] are also important for quark confinement, and then it might be interesting to investigate those in terms of the Dirac mode expansion.

In the above discussion, the Dirac operator is taken to have the naive form. Then, the analytical relation should be generalized to the proper Dirac operator on the lattice. However, it is difficult to directly derive the analytical relations connecting the Polyakov loop and the overlap-Dirac eigenmodes. Thus, we first derive the analytical relation between the Polyakov loop and the Wilson-Dirac operator. Using the relation, we conclude that the confinement property is independent of the low-lying mode density of the overlap-Dirac operator. Strictly speaking, the Wilson-Dirac modes are not complete system, and thus the above argument is approximately valid. However, the Wilson-Dirac operator is almost anti-hermite, and the hermitian term is $\mathcal{O}(a)$. Therefore, the result is expected to be exact in the continuum limit.

Our study consistently indicates no direct one-to-one correspondence between quark-confinement and chiral symmetry breaking in QCD. However, there are some opposite findings. That is, they suggest some strong correlation between these non-perturbative phenomena. Unfortunately, this contradiction has not been sufficiently explained yet. A solution for this controversial problem is to find a new phase where quarks are confined but the chiral symmetry is restored. If the new phase exists, it means that confinement and chiral symmetry breaking can independently occur in QCD.

Although the new phase does not exist at finite temperature, it might appear at finite chemical potential, or under the external fields, for instance, magnetic fields [86]. In particular, the phase structure of QCD attracts much attention in the context of the internal structure of neutron stars because an extreme state with high density and low temperature is expected to be realized there. However, the first-principle calculation is prevented by the sign problem at finite chemical potential, in particular large chemical potential [87, 88, 89, 90]. Recently, the sign problem is being solved thanks to development of new techniques [91, 92, 93, 94, 95]. When the first principle calculation is available for $SU(3)_c$ QCD at finite temperature and chemical potential, we can more deeply understand the phase structure of QCD and then the relations between the nonperturbative phenomena, such as confinement and chiral symmetry breaking.

Acknowledgements

I would like to thank my supervisor, Hideo Suganuma for useful discussion and great guidance. I also thank to my collaborators, Takumi Iritani, Krzysztof Redlich, and Chihiro Sasaki in the studies reported in this thesis, and Nodoka Yamanaka, Shotaro Imai, and Shoichiro Tsutsui in the other works. I am grateful for all the member of the nuclear theory group in Kyoto university and Yukawa Institute for Theoretical Physics for much advise and support.

This work is supported by the Grant-in-Aid for JSPS fellows (No.15J02108). The lattice QCD calculations have been performed on NEC-SX8R and NEC-SX9 at Osaka university.

Appendix A

The relation between the Dirac matrix element and the KS Dirac matrix element

The relations between the Dirac matrix element and the KS Dirac matrix element are shown in both even and temporally odd-number lattices.

A.1 The case of the even lattice

First, the even lattice and the original KS formalism is considered. Using the relation between the Dirac eigenfunction ψ and the KS-Dirac eigenfunction χ, the Dirac matrix element of a link variable operator $\langle n, I|\hat{U}_\mu|m, J\rangle$ is expressed as

$$\begin{aligned}
&\langle n, I|\hat{U}_\mu|m, J\rangle \\
&= \sum_{s,\alpha} \psi_n^I(s)^\dagger_\alpha U_\mu(s)\psi_m^J(s+\hat{\mu})_\alpha \\
&= \sum_{s,\alpha} \chi_n(s)^\dagger T^\dagger(s)_{I\alpha} U_\mu(s) T(s+\hat{\mu})_{\alpha J}\chi_m(s+\hat{\mu}) \\
&= \sum_{s} \chi_n(s)^\dagger \{T^\dagger(s)T(s+\hat{\mu})\}_{IJ} U_\mu(s)\chi_m(s+\hat{\mu}).
\end{aligned} \tag{A.1}$$

From the direct calculation, the matrix $T^\dagger(s)T(s+\hat{\mu})$ is calculated from the definition of the matrix $T(s)$ (2.25):

$$T^\dagger(s)T(s+\hat{\mu}) = \tilde{\eta}_\mu^{(\mathrm{E})}(s)\gamma_\mu, \tag{A.2}$$

where $\tilde{\eta}_\mu^{(\mathrm{E})}(s)$ is a sign function defined as

$$\tilde{\eta}_\mu^{(\mathrm{E})}(s) = (-1)^{s_{\mu+1}+\cdots+s_4} \ (\mu \leq 3), \qquad \tilde{\eta}_4^{(\mathrm{E})}(s) = 1, \tag{A.3}$$

which is similar to the staggered phase (2.27). Then, the Dirac matrix element is expressed as

$$\begin{aligned}
&\langle n, I|\hat{U}_\mu|m, J\rangle \\
&= (\gamma_\mu)_{IJ} \sum_s \tilde{\eta}_\mu^{(\mathrm{E})}(s)\chi_n(s)^\dagger U_\mu(s)\chi_m(s+\hat{\mu}) \\
&= (\gamma_\mu)_{IJ}(n|\hat{\tilde{\eta}}_\mu^{(\mathrm{E})}\hat{U}_\mu|m),
\end{aligned} \tag{A.4}$$

where $\hat{\tilde{\eta}}_\mu^{(\mathrm{E})}$ is an operator defined as

$$\langle s|\hat{\tilde{\eta}}_\mu^{(\mathrm{E})}|s'\rangle = \tilde{\eta}_\mu^{(\mathrm{E})}(s)\delta_{ss'} \tag{A.5}$$

corresponding to the sign function $\tilde{\eta}_\mu^{(\mathrm{E})}(s)$. In particular, since $\tilde{\eta}_4^{(\mathrm{E})}(s) = 1$ is satisfied for $\mu = 4$, we obtain

$$\langle n, I|\hat{U}_4|m, J\rangle = (\gamma_4)_{IJ}(n|\hat{U}_4|m). \tag{A.6}$$

Here we consider only the Dirac matrix element of one link-variable operator $\langle n, I|\hat{U}_\mu|m, J\rangle$. However, that of other operator consisting of link-variable operators $\langle n, I|\hat{O}(\hat{U})|m, J\rangle$ can be evaluated in terms of the KS Dirac matrix element or the KS Dirac eigenfunction $\chi_n(s)$ by similar calculation on the even lattice.

A.2 The case of the temporally odd-number lattice

Next, the temporally odd-number lattice and the modified KS formalism are considered. Corresponding to the even lattice, the Dirac matrix element of a link variable operator $\langle n, I|\hat{U}_\mu|m, J\rangle$ is expressed as

$$\begin{aligned}
&\langle n, I|\hat{U}_\mu|m, J\rangle \\
&= \sum_{s,\alpha} \psi_n^I(s)_\alpha^\dagger U_\mu(s)\psi_m^J(s+\hat{\mu})_\alpha \\
&= \sum_{s,\alpha} \chi_n(s)^\dagger M^\dagger(s)_{I\alpha} U_\mu(s) M(s+\hat{\mu})_{\alpha J}\chi_m(s+\hat{\mu}) \\
&= \sum_s \chi_n(s)^\dagger \{M^\dagger(s)M(s+\hat{\mu})\}_{IJ} U_\mu(s)\chi_m(s+\hat{\mu})
\end{aligned} \tag{A.7}$$

Like the case of the Eq.(A.2), $M^\dagger(s)M(s+\hat{\mu})$ can be calculated as

$$M^\dagger(s)M(s+\hat{\mu}) = \tilde{\eta}_\mu^{(\mathrm{O})}(s)\gamma_\mu\gamma_4, \tag{A.8}$$

where $\tilde{\eta}_\mu^{(\mathrm{O})}(s)$ is a different sign function defined as

$$\tilde{\eta}_\mu^{(\mathrm{O})}(s) = (-1)^{s_1+\cdots+s_\mu}\ (\mu \leq 3), \qquad \tilde{\eta}_4^{(\mathrm{O})}(s) = 1. \tag{A.9}$$

Using this fact, the Dirac matrix element can be written as

$$\begin{aligned}
&\langle n, I|\hat{U}_\mu|m, J\rangle \\
&= (\gamma_\mu\gamma_4)_{IJ}\sum_s \tilde{\eta}_\mu^{(\mathrm{O})}(s)\chi_n(s)^\dagger U_\mu(s)\chi_m(s+\hat{\mu}) \\
&= (\gamma_\mu\gamma_4)_{IJ}(n|\hat{\tilde{\eta}}_\mu^{(\mathrm{O})}\hat{U}_\mu|m),
\end{aligned} \tag{A.10}$$

where $\hat{\tilde{\eta}}_\mu^{(\mathrm{O})}$ is an operator defined as

$$\langle s|\hat{\tilde{\eta}}_\mu^{(\mathrm{O})}|s'\rangle = \tilde{\eta}_\mu^{(\mathrm{O})}(s)\delta_{ss'} \tag{A.11}$$

corresponding to the sign function $\tilde{\eta}_\mu^{(\mathrm{E})}(s)$. In particular, since $\tilde{\eta}_4^{(\mathrm{O})}(s) = 1$ is satisfied for $\mu = 4$, we obtain

$$\langle n, I|\hat{U}_4|m, J\rangle = \delta_{IJ}(n|\hat{U}_4|m). \tag{A.12}$$

For more special case, the diagonal component $\langle n, I|\hat{U}_4|n, I\rangle$ is expressed as

$$\langle n, I|\hat{U}_4|n, I\rangle = (n|\hat{U}_4|n). \tag{A.13}$$

This is used in chapter 2 in this thesis.

Like the case of the even lattice, one can evaluate the Dirac matrix element of the other operator $\langle n, I|\hat{O}(\hat{U})|m, J\rangle$, using the KS Dirac matrix element or the KS Dirac eigenfunction $\chi_n(s)$ on the temporally odd-number lattice.

Bibliography

[1] M.E. Peskin and D.V. Schroeder, *An Introduction to Quantum Field Theory*, Perseus Books, 1995.

[2] C. N. Yang and R. L. Mill, Phys. Rev. **96**, 191 (1954).

[3] D.J. Gross and F. Wilczek, Phys. Rev. Lett. **30**, 1343 (1973).

[4] H. D. Politzer, Phys. Rev. Lett. **30**, 1346 (1973).

[5] J. Greensite, *An Introduction to the Confinement Problem*, Springer, 2011.

[6] E. Eichten, K. Gottfried, T. Kinoshita, J. Kogut, K. D. Lane, and T. M. Yan, Phys. Rev. Lett. **34**, 369 (1975); Phys. Rev. Lett. **36**, 1276 (1976).

[7] G. S. Bali, K. Schilling and C. Schlichter, Phys. Rev. D **51**, 5165 (1995).

[8] G. S. Bali, Phys. Rept. **343**, 1 (2001).

[9] H. Ichie, V. Bornyakov, T. Streuer and G. Schierholz, Nucl. Phys. **A721**, 899 (2003).

[10] T.T. Takahashi, H. Suganuma, H. Ichie, H. Matsufuru and Y. Nemoto, Nucl. Phys. **A721**, 926 (2003).

[11] V.G. Bornyakov et al. [DIK Collaboration], Phys. Rev. D **70**, 054506 (2004).

[12] H.J. Rothe, *Lattice Gauge Theories*, World Scientific, 2012.

[13] L.D. McLerran and B. Svetitsky, Phys. Rev. D **24**, 450 (1981).

[14] Y. Nambu, Phys. Rev. D **10**, 4262 (1974).

[15] G. 't Hooft, in *Proceedings of High Energy Physics*, Editrice Compositori 1976.

[16] S. Mandelstam, Phys. Rep. C **23**, 245 (1976).

[17] G. 't Hooft, Nucl. Phys. **B190**, 455 (1981).

[18] H. Suganuma, S. Sasaki and H. Toki, Nucl. Phys. **B435**, 207 (1995).

[19] O. Miyamura, Phys. Lett. B **353**, 91 (1995).

[20] R.M. Woloshyn, Phys. Rev. D**51**, 6411 (1995).

[21] N. Sakumichi, H. Suganuma, Phys.Rev. D**90** 111501 (2014).

[22] Y.M. Cho, F.H. Cho and J.H. Yoon, Phys. Rev. D **87**, 085025 (2013).

[23] L. Faddeev and A. Niemi, Phys. Rev. Lett. **82**, 1624 (1999).

[24] S. Kato, K. Kondo, T. Murakami, A. Shibata, T. Shinohara and S. Ito, Phys. Lett. B **632**, 326 (2006).

[25] T. Kugo and I. Ojima, Prog. Theor. Phys. Suppl. **66**, 1 (1979).

[26] S. Furui, H. Nakajima, Phys.Rev. D**69** 074505 (2004).

[27] N. Yamanaka, T.M. Doi, S. Imai and H. Suganuma, Phys. Rev. D**88** 074036 (2013).

[28] N. Yamanaka, S. Imai, T.M. Doi and H. Suganuma, Phys. Rev. D**89**, 074017 (2014).

[29] Y. Nambu and G. Jona-Lasinio, Phys. Rev. **122**, 345 (1961); **124**, 246 (1961).

[30] J. Goldstone, Nuovo Cim. **19**, 154 (1961).

[31] J. Goldstone, A. Salam and S. Weinberg, Phys. Rev. **127**, 965 (1962).

[32] T. Banks and A. Casher, Nucl. Phys. **B169** (1980) 103.

[33] K.G. Wilson, Phys. Rev. D **10**, 2445 (1974).

[34] M. Creutz, *Quarks, Gluons and Lattices*, Cambridge University Press, 1983.

[35] H.B. Nielsen and M. Ninomiya, Nucl. Phys. **B185**, 20 (1981).

[36] H.B. Nielsen and M. Ninomiya, Nucl. Phys. **B193**, 173 (1981).

[37] M. G. Alford, K. Rajagopal, F. Wilczek, Phys. Lett. B**422**, 247 (1998).

[38] M. G. Alford, K. Rajagopal, F. Wilczek, Nucl. Phys. B**537**, 443 (1999).

[39] R. Rapp, T. Schaefer, E. V. Shuryak, M. Velkovsky, Phys. Rev. Lett. **81**, 53 (1998).

[40] K. Fukushima and C. Sasaki, Prog. Part. Nucl. Phys. **72**, 99 (2013).

[41] K. Fukushima, T. Hatsuda, Rept. Prog. Phys. **74**, 014001 (2011).

[42] Z. Fodor and S.D. Katz, Phys. Lett. B**534**, 87 (2002).

[43] D.T. Son and Misha A. Stephanov, Phys. Rev. Lett. **86**, 592 (2001).

[44] P. de Forcrand and O. Philipsen, Nucl. Phys. B**642**, 290 (2002).

[45] S. Muroya, A. Nakamura, C. Nonaka, and T. Takaishi, Prog. Theor. Phys. **110**, 615 (2003).

[46] C. Gattringer, Phys. Rev. Lett. **97**, 032003 (2006).

[47] F. Bruckmann, C. Gattringer and C. Hagen, Phys. Lett. B **647**, 56 (2007).

[48] E. Bilgici, F. Bruckmann, C. Gattringer, and C. Hagen, Phys. Rev. D**77**, 094007 (2008).

[49] Y. Hatta and K. Fukushima, Phys. Rev. D**69**, 097502 (2004).

[50] C.B. Lang and M. Schrock, Phys. Rev. D**84**, 087704 (2011). L.Ya. Glozman, C.B. Lang, and M. Schrock, Phys. Rev. D**86**, 014507 (2012).

[51] S. Gongyo, T. Iritani and H. Suganuma, Phys. Rev. D **86**, 034510 (2012).

[52] T. Iritani and H. Suganuma, PTEP **2014**, 033B03 (2014).

[53] F. Synatschke, A. Wipf and K. Langfeld, Phys. Rev. D**77**, 114018 (2008).

[54] J. Kogut, M. Stone, H.W. Wyld, W.R. Gibbs, J. Shigemitsu, S.H. Shenker and D.K. Sinclair,
Phys. Rev. Lett. **50**, 393 (1983).

[55] F. Karsch, Lect. Notes Phys. **583**, 209 (2002).

[56] J.D. Stack, S.D. Neiman, and R.J. Wensley, Phys. Rev. D**424** 50, 3399 (1994).

[57] H. Suganuma, A. Tanaka, S. Sasaki, and O. Miyamura, Nucl. Phys. B**47** Proc. Suppl., 302 (1996).

[58] Y. Aoki, Z. Fodor, S.D. Katz and K.K. Szabo, Phys. Lett. B**643**, 46 (2006).

[59] Y. Aoki, S. Borsanyl, S. Durr, Z. Fodor, S.D. Katz, S. Krieg and K.K. Szabo, JHEP**06**, 088 (2009).

[60] T. Bhattacharya et.al. Phys. Rev. Lett. **113**, 082001 (2014).

[61] T. M. Doi, H. Suganuma, T. Iritani, Phys. Rev. D**90**, 094505 (2014).

[62] H. Suganuma, T. M. Doi, T. Iritani, PTEP **2016**, 013B06 (2016).

[63] S. Elitzur, Phys. Rev. D **12**, 3978 (1975).

[64] J.B. Kogut and L. Susskind, Phys. Rev. D**11**, 395 (1975).

[65] E. Anderson *et al.*, LAPACK Users' Guide, Third, (Society for Industrial and Applied Mathematics, 1999).

[66] T. M. Doi, K. Redlich, C. Sasaki, H. Suganuma, Phys. Rev. D**92**, 094004 (2015).

[67] G. Boyd, J. Engels, F. Karsch, E. Laermann, C. Legeland, M. Lutgemeier, and B. Petersson, Phys. Rev. Lett. **75** (1995) 4169.

[68] G. Boyd, J. Engels, F. Karsch, E. Laermann, C. Legeland, M. Lutgemeier, and B. Petersson, Nucl. Phys. B **469** (1996) 419.

[69] S. Borsanyi, G. Endrodi, Z. Fodor, S. D. Katz, and K. K. Szabo, JHEP **1207** (2012) 056.

[70] F. R. Brown, F. P. Butler, H. Chen, N. H. Christ, Z. Dong, W. Schaffer, Leo I. Unger and Alessandro Vaccarino, Phys. Rev. Lett. **65**, 2491 (1990).

[71] R. D. Pisarski and F. Wilczek, Phys. Rev. D**29**, 338 (1984).

[72] E. Laermann and O. Philipsen, Ann. Rev. Nucl. Part. Sci. **53**, 163 (2003).

[73] A. Bazavov, T. Bhattacharya, M. Cheng, C. DeTar, H. T. Ding, S. Gottlieb, R. Gupta and P. Hegde *et al.*, Phys. Rev. D**85**, 054503 (2012).

[74] A. Bazavov *et al.* [HotQCD Collaboration], Phys. Rev. D**90**, 094503 (2014).

[75] P.M. Lo, B. Friman, O. Kaczmarek, K. Redlich and C. Sasaki, Phys. Rev. D**88**, 014506 (2013).

[76] P.M. Lo, B. Friman, O. Kaczmarek, K. Redlich and C. Sasaki, Phys. Rev. D**88**, 074502 (2013).

[77] M. Creutz and K.J.M. Moriarty, Phys. Rev. D**26**, 2166 (1982).

[78] P.H. Ginsparg and K.G. Wilson, Phys. Rev. D**25**, 2649 (1995).

[79] H. Neuberger, Phys. Lett. B**417**, 141 (1998).

[80] H. Neuberger, Phys. Lett. B**427**, 353 (1998).

[81] M. Luscher, Phys. Lett. B**428**, 342 (1998).

[82] S. Aoki et al., Phys. Rev. D**78**, 014508 (2008).

[83] S. Ejiri, F. Karsch and K. Redlich, Phys. Lett. B**633**, 275 (2006).

[84] C. Schmidt [BNL-Bielefeld Collaboration], Nucl. Phys. A**904-905**, 865c (2013).

[85] C. Sasaki, Nucl. Phys. A**931**, 238 (2014).

[86] H. Suganuma and T. Tatsumi, Ann. Phys. **208**, 470 (1991); Prog. Theor. Phys. **90**, 379 (1993).

[87] E.Y. Loh, J.E. Gubernatis, R.T. Scalettar, S.R. White, D.J. Scalapino, R.L. Sugar, Phys. Rev. B**41**, 9301(1990).

[88] W. von der Linden, Physics Reports **220**, 53 (1992).

[89] S. Muroya, A. Nakamura, C. Nonaka, and T. Takaishi, Prog. Theor. Phys. **110**, 615 (2003).

[90] P. de Forcrand, PoS LAT2009, 010 (2009).

[91] E. Seiler, D. Sexty, I.-O. Stamatescu, Phys. Lett. B**723**, 213 (2013).

[92] M. Cristoforetti, F. Di Renzo, and L. Scorzato, Phys. Rev. D**86**, 074506 (2012).

[93] H. Fujii, D. Honda, M. Kato, Y. Kikukawa, S. Komatsu, T. Sano, JHEP **1310**, 147 (2013).

[94] K. Nagata, J. Nishimura, S. Shimasaki, PTEP **2016**, 013B01 (2016).

[95] S. Tsutsui, T. M. Doi, Phys. Rev. D**94**, 074009 (2016).